



## Article

# Using Optical Water-Type Classification in Data-Poor Water Quality Assessment: A Case Study in the Torres Strait †

Caroline Petus <sup>1,\*</sup>, Jane Waterhouse <sup>1</sup>, Dieter Tracey <sup>1</sup>, Eric Wolanski <sup>2</sup> and Jon Brodie <sup>3</sup>

<sup>1</sup> Catchment to Reef Research Group, TROPWATER, James Cook University, Townsville, QLD 4811, Australia; jane.waterhouse@jcu.edu.au (J.W.); dieter.tracey@jcu.edu.au (D.T.)

<sup>2</sup> College of Science and Engineering, James Cook University, Townsville, QLD 4811, Australia; eric.wolanski@jcu.edu.au

<sup>3</sup> Formerly ARC Centre of Excellence for Coral Reef Studies, James Cook University, Townsville, QLD 4811, Australia; jon.brodie@jcu.edu.au

\* Correspondence: caroline.petus@jcu.edu.au

† This work is dedicated to the memory of our dear colleague Jon Brodie who was the science leader of this project.

**Abstract:** For many years, local communities have expressed concerns that turbid plume waters from the Fly River in Papua New Guinea may potentially deliver mine-derived contaminants to the Torres Strait, an ecologically and culturally unique area north of the Australian mainland. Information on suspended sediment transport and turbidity patterns are needed in this data-limited region to identify and manage downstream ecosystems that may be at risk of exposure from the Fly River runoff. This study used MODIS satellite time series and a colour-classification approach to map optical water types around the data-poor Gulf of Papua and Torres Strait region. The satellite data were supported by field data, including salinity and suspended sediment measurements, and used together in qualitative water quality assessments to evaluate the habitats that are likely exposed to Fly River discharge and/or derived sediments. It showed that the Fly River influence in the Torres Strait region is largely limited to the north-east corner of the Torres Strait. The drivers of turbidity vary between locations, and it is impossible to fully separate direct riverine plume influence from wave and tidally driven sediment resuspension in the satellite maps. However, results indicate that coastal habitats located as far east as Bramble Cay and west to Boigu Island are located in an area that is most likely exposed to the Fly River discharge within the region, directly or through sediment resuspension. The area that is the most likely exposed is a relatively small proportion of the Torres Strait region, but encompasses habitats of high ecological importance, including coral reefs and seagrass meadows. Satellite data showed that the period of highest risk of exposure was during the south-east trade wind season and complemented recent model simulations in the region over larger spatial and temporal frames. This study did not evaluate transboundary pollution or the ecological impact on local marine resources, but other recent studies suggest it is likely to be limited. However, this study did provide long-term, extensive but qualitative, baseline information needed to inform future ecological risk mapping and to support decision making about management priorities in the region. This is important for ensuring the protection of the Torres Strait ecosystems, given their importance to Torres Strait communities and turtle and dugong populations, and the Torres Strait's connectivity with the Great Barrier Reef Marine Park.

**Keywords:** Torres Strait; Fly River plume; suspended sediment concentration; satellite imagery; colour scales; MODIS; Sentinel-3; exposure assessment; Great Barrier Reef



**Citation:** Petus, C.; Waterhouse, J.; Tracey, D.; Wolanski, E.; Brodie, J. Using Optical Water-Type Classification in Data-Poor Water Quality Assessment: A Case Study in the Torres Strait. *Remote Sens.* **2022**, *14*, 2212. <https://doi.org/10.3390/rs14092212>

Academic Editor: Chris Roelfsema

Received: 20 December 2021

Accepted: 18 April 2022

Published: 5 May 2022

**Publisher's Note:** MDPI stays neutral with regard to jurisdictional claims in published maps and institutional affiliations.



**Copyright:** © 2022 by the authors. Licensee MDPI, Basel, Switzerland. This article is an open access article distributed under the terms and conditions of the Creative Commons Attribution (CC BY) license (<https://creativecommons.org/licenses/by/4.0/>).

## 1. Introduction

Increased sediment and contaminant loads from riverine runoff are a significant threat to the health of nearshore and marine ecosystems worldwide [1–3] and can also increase

vulnerability to climate change stress [4–6]. Protection of marine ecosystems requires water quality issues to be addressed through marine conservation and run-off management in adjacent catchments [7,8], supported by spatially explicit information on how, when and where land-based sediments and contaminants are transported and on which ecosystems are likely to be exposed and to be at ecological risk from land-based runoff [9–14]. This information is particularly challenging and costly to gather in remote tropical marine environments, where field data are scarce and complicated to collect due to geographical, logistical, administrative and weather-related obstacles [15] or, more generally, in large-scale ecosystems where data at the right spatial and/or temporal scales are missing to address the scale and complexity of ridge-to-reef environments [16]. In these challenging environments, satellite images provide unique spatial coverage and temporal frequencies to fill in gaps in observed data. They provide essential baseline water quality information, which, when combined with modelling and/or field measurements, can be used to inform management and conservation strategies [13,14,17–20].

This study focused on the Torres Strait (TS), an ecologically and culturally unique area located at the northernmost extent of the Great Barrier Reef (GBR) (Figure 1a). The region is potentially threatened by runoff from adjacent mining activities in Papua New Guinea (PNG). Several rivers drain the southern PNG coast, including the Fly River, which accounts for about half the PNG total river discharge ( $\sim 6000 \text{ m}^3 \text{ s}^{-1}$ ) [21]. It is the 17th-largest river in the world in terms of sediment discharge and creates a large brownish river plume in the Gulf of Papua (Figure 1b) [22,23]. The Ok Tedi copper mine has been operating in the headwaters of the Fly River since 1984 (Figure 1a). It discharges contaminated sediments in the form of mine tailings into the Fly River, which ultimately flow into the Fly River Delta and the Gulf of Papua. This has caused extensive damage to the Fly River system, including contamination of the water and sediment by copper [24,25], increased turbidity levels [21] and changes to river geomorphology through sediment deposition [22,26,27]. Increased copper concentrations have been measured downstream on the Fly Delta sediments [28], and mining is estimated to have caused a 40% increase in the sediment discharge from  $85 \text{ Mt y}^{-1}$  to  $120 \text{ Mt y}^{-1}$  [21]. Given the close proximity of TS to the Fly River estuary mouth, local communities have been raising concerns that PNG runoff may deliver contaminants to the TS marine environment since the start of mine operations [22,26,27].

A large proportion of sediments from the Fly River are retained in the delta through flocculation [23,29] or transported in the Gulf of Papua [30]. However, under certain oceanographic conditions a small fraction of the Fly River plume waters can be entrained in the TS as suspended sediments. Turbid riverine waters from PNG have occasionally been observed in the north-east corner of the TS in the field [31] and on satellite images (Figure 1b) [32,33], but no long-term analysis of turbidity patterns in the region has been performed.

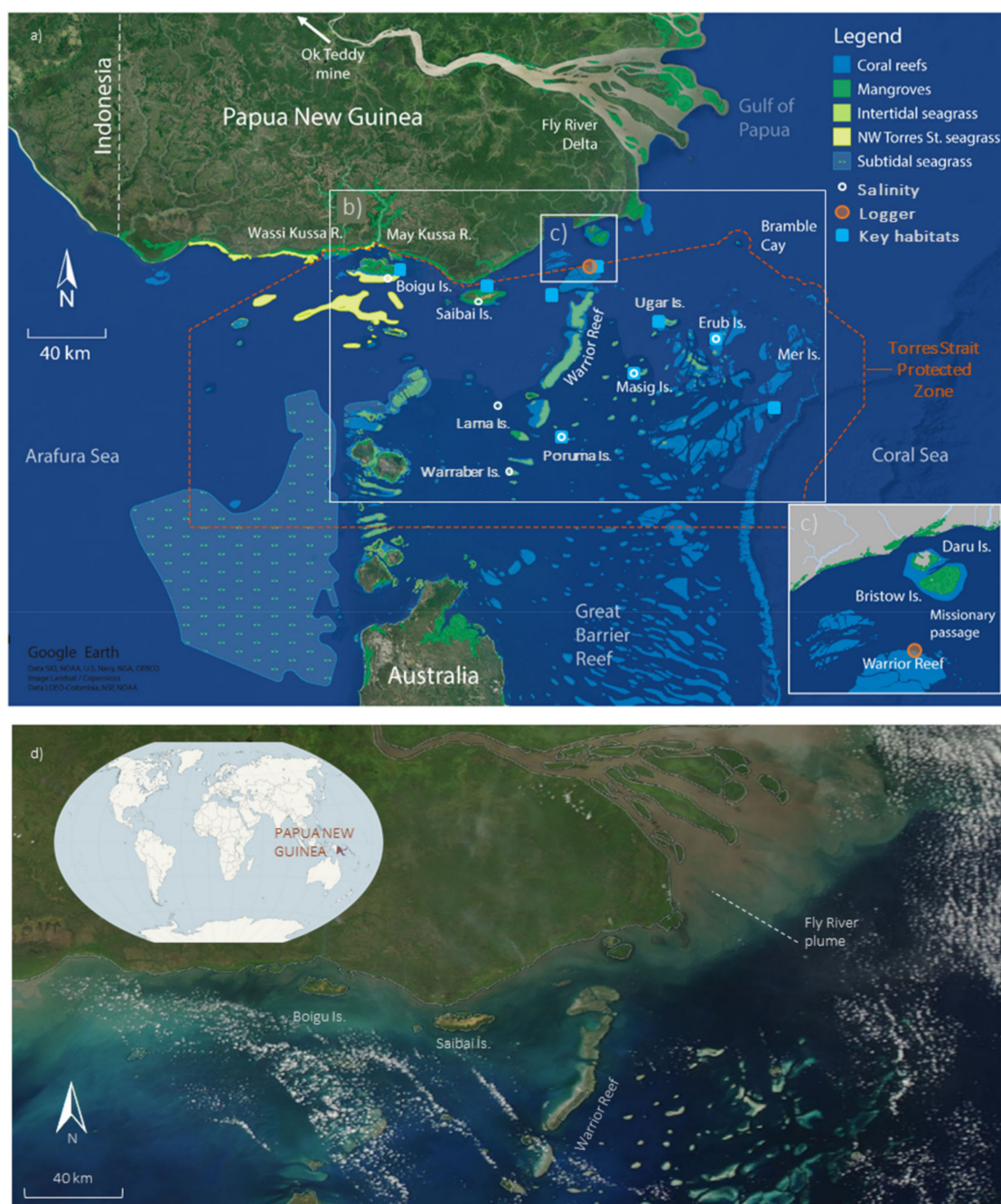


**Figure 1.** (a) Map of the TS region showing the major rivers, islands, the boundary of the TS Protected Zone, and the TS habitats (mapped coral reefs [34], intertidal and subtidal seagrass [35], North-West TS seagrass [36]) ([22], modified). TS habitats assessed in this study are indicated with blue square symbols, collected salinity data with a yellow circle and the location of the loggers with an orange circle. (b) Exposure assessment area and (c) zoom to Daru Island. (d) MODIS-Aqua true colour image of the 12 October 2016 showing the Fly River plume and a general location map. The image is from the NASA Worldview application and shows a large brownish river plume off the Fly River Delta.

Physical models of the region suggest that Fly River sediments intrude when the prevailing current is westward, i.e., largely during the south-east (SE) trade wind season [23,37], and 2% to 11% of the sediment discharged by the Fly River has been estimated to be deposited in the TS [23,38]. These models have not, however, been fully validated due to a lack of observational data at sufficient spatial and temporal resolutions [23,37]. Intrusion of the Fly River plume in the TS is a natural process that occurred for several thousands

of years before mining started. Transported suspended sediments generally settle during calm weather and are resuspended by tidal currents, wind and waves and have formed a continuous mud wedge about 20 km wide all along the PNG coast (hereafter TS mud wedge) [23]. However, the mining activities are suspected to have changed these sediment dynamics and the spatial extent of the Fly River runoff. Variations in Fly River discharge and plume movements have also been linked to tidal fluctuations (semidiurnal cycles) and the El Niño-Southern Oscillation (ENSO) cycles (inter-annual cycles) [39–41] but are not fully understood.

This study was part of a collaborative research project funded by the Australian Government as part of the National Environmental Science Program Tropical Water Quality Hub (NESP-TWQ Projects 2.2.1, 2.2.2 and 5.14) [22,26,27,42]. The project applied a multiple-lines-of-evidence approach to assess the likely influence of the Fly River discharge on the TS [22]. The project components included a field water-quality component [42], a modelling component [23,41], analyses of historical coral core records [43] and a remote sensing component (this study). Specifically, the remote sensing component aimed to further understand turbidity patterns in the region and identify TS habitats likely exposed to Fly River runoff using publicly available satellite images. This remote sensing component is the focus of this paper.

Suspended sediment concentrations (SSC, in  $\text{mg L}^{-1}$ ) or turbidity levels (in NTU) can be quantified in large-scale marine areas using optical satellite imageries and empirical or physical bio-optical algorithms, e.g., [44,45]. However, there is very limited knowledge of the bio-optical properties of particulate and dissolved substances in the optically complex TS coastal waters, which greatly limits the development of accurate ocean colour models for the TS region [46,47]. The lack of optical field data, as well as the challenges of collecting new data in this remote area, also limit the ability to confidently validate, parameterise and/or regionally-tune global algorithms or algorithms developed for other optical settings to the TS region.

To overcome these limitations, this study focused on a qualitative method of analysis, whereby the colour of the water retrieved from optical satellite imageries was used to classify TS water into optical water types (OWTs) with distinctly characteristic turbidity levels [48]. Water colour is the result of the presence of marine constituents (SSC, chlorophyll-a [Chl-a] and coloured dissolved organic matter [CDOM]) and their interactions with solar irradiance [49]. Several studies have reported that there is a quantifiable relationship between water colour and water quality parameters, including a strong relationship with turbidity [50–52]. Accordingly, water colour is regarded as a simple yet efficient optical parameter for assessing water quality changes [14,53]. It has been used worldwide, including in the GBR, to assess water quality changes related to different turbidity levels, SSC and Chl-a concentrations, and Secchi Disk Depth in inland and marine waters [14,50,54–58]. Importantly, water colour classification algorithms do not require a full characterisation of regional optical properties using local in situ water quality data and are thus suited to data-limited study areas [50].

The assessment of water colour was supported by other evidence collected through the NESP-TWQ program, including field salinity and SSC data [26,27,42], results of recent hydrodynamic and sediment transport modelling [23,41], and the coral core analyses [43], as well as other historical evidence published in the literature. These different datasets were used together in a qualitative water quality assessment and provided spatially explicit information for when and where the influence from Fly River discharge is likely to occur and identified which TS zones and habitats are the most likely to be exposed. It is impossible to fully separate the direct influence of riverine plume from wind, wave and tidally driven sediment resuspension (some of which may have been originally derived from the Fly River discharge) in optical satellite images. In this study, the exposure is thus defined as “exposure to turbid waters from or derived from the Fly River”.

## 2. Study Area

The TS stretches 200 km from the northern tip of the Cape York Peninsula to the south-west coast of PNG in the south-western Pacific Ocean north of Australia (Figure 1a). There are more than 300 islands and cays in the TS, 17 of which are inhabited and support an estimated 8700 people [59]. The TS Protected Zone established under the TS Treaty (Figure 1a) protect the traditional way of life of TS Islanders between international boundaries. The TS has large areas of diverse coral reefs, extended areas of coastal mangroves and productive fisheries, and the largest continuous area of seagrass meadows in the world [59] (Figure 1a). The region's variety of habitats supports highly diverse Indo-Pacific marine flora and fauna, including dugongs and marine turtles [60,61]. The coral reefs of the TS are adjacent to the far northern section of the GBR Marine Park and provide ecological functions that influence the broader GBR [62]. The TS is situated in a wet tropical region, and the climate is dominated by alternating periods of monsoon and SE trade winds. The primary characteristics of these seasons are summarised in Table 1.

**Table 1.** Summary of the METocean and hydrodynamic characteristics of the PNG region [23,38,39,41,43,63].

Characteristics	Monsoon Season	Trade Wind Season
Time period	January to April	May to December:
Winds	NW monsoon—Typical wind speeds in the area are of order 9 knots	SE trade winds—typical wind speeds of over 20 knots. A period of relative calm (transition period) occurs between November and December with winds slowly veering and backing to northerly.
Waves	Offshore winds result in little or no long-period swell propagating towards the south coast of PNG.	TS is generally protected from surface waves by the northern-most extension of the GBR
Rainfall	Higher rainfall (median December–May = 1968 mm). Storms and infrequent tropical cyclones influence the inter-annual variability of the sediment fluxes	Lower rainfall (median June–November = 1345 mm)
Wind-driven currents	Eastward	Westward. Controls the westward transport of suspended sediments along the southern coast of PNG between Daru and Saibai Island.
Mean sea level (MSL) difference across the TS	Negative (MSL Gulf of Carpentaria > MSL Gul of Papua)	Positive (MSL Gulf of Carpentaria < MSL Gulf of Papua)

The Fly River is the largest sediment source of the study area. It delivers sediment to the south coast of PNG relatively invariantly throughout the year, with minimal seasonal fluctuations [21]. Rivers located along the southern PNG coastline (Irian Jaya), including the Wassi Kussa and Mai Kussa Rivers, also flow into the TS region, although they are considerably smaller (Figure 1a). Sediment mobility is dominated by waves in the Gulf of Papua and by a mixture of waves and tides in TS [63]. During the SE trade winds, the TS is generally protected from surface waves generated in the Coral Sea by the northern-most extension of the GBR, serving to block swell while the Fly River Delta remains exposed to Coral Sea-generated swell (Table 1) [38,63]. During the NW monsoon, offshore winds result in little or no long-period swell propagating towards the south coast of PNG and the inter-annual variability of the sediment fluxes during the monsoon has been attributed to storms and remote cyclone impacts [38]. The TS forms the intersection of two separate and dissimilar tidal regimes of the Gulf of Papua/Coral Sea and the Gulf of Carpentaria/Arafura Sea (Figure 1a). These phenomena drive strong, highly dynamic

tidal currents magnified by flow channelisation in passages among dense coral reefs through the TS. Wind-driven currents are observed to reverse seasonally, with flow being generally westwards during the SE trade wind season and eastwards during the NW monsoon [20,23,41] (Table 1 and Appendix A, Figure A1).

### 3. Materials and Method

#### 3.1. Satellite Data

OWT maps of the study area were produced using a colour classification scheme developed originally for the GBR: the wet season (WS) colour scale for MODIS-Aqua (MA) satellite images [14,17,20,48]. The WS colour scale divides water into 7 WS colour classes, ranging in colour from brownish to bluish, corresponding to four broad OWTs (Table 2). These OWTs represent typical colour and turbidity gradients encountered in the GBR during the wet season (December to April), including riverine plumes [14,17,20,48]. OWTs are classified depending on water colour and linked to water quality characteristics (Table 2). ‘Primary waters’ (or WS1–4) are brownish waters, enriched in sediment and dissolved organic matter, and ‘Secondary waters’ (or WS5) are greenish waters, enriched in algae and dissolved organic matter and with a relatively lower suspended sediment content. ‘Tertiary waters’ (WS6) are greenish-blue and the marine OWT (WS7) blueish, and both correspond to waters with higher light penetration [14,17,20,48]. SSC and turbidity levels typically decrease from the Primary to the Tertiary OWT (Table 2). The Primary water type is often associated with low salinity from river discharge but can also reflect re-suspended sediment from wind and tides. The Secondary water type is often associated with relatively less turbid water and is typically found in the open coastal waters and outer flood plume waters of the GBR. Tertiary and marine waters are found in the midshelf and offshore waters of the GBR and have a low risk of detrimental ecological effects [20].

**Table 2.** Comparison between WS and FU OWTs and long-term SCC and SDD concentrations measured in the GBR [modified from 14,20].

Water Colour	WS Colour Scale (GBR) OWT Name (WS Colour Classes)	FU Colour Scale (Global) OWT Name (FU Colour Classes)	Description	SCC (mg L <sup>-1</sup> ) and SDD (m) Measured in the GBR
Brownish to brownish-green	Primary (WS1-4)	Primary’ (FU ≥ 10)	Turbid waters with high SSC, but also enriched in chl-a, and CDOM resulting in reduced light levels. In the GBR, this OWT is typical of inshore regions that receive land-based discharge and have high concentrations of resuspended sediments during the wet season.	SCC: 18.3 ± 45.7 mg L <sup>-1</sup> and SDD: 1.8 ± 1.7 m
Greenish to greenish-blue	Secondary (WS5)	Secondary’ (FU6-9)	Less turbid water typical of coastal waters rich in algae (Chl-a) and containing CDOM and fine sediment. In the GBR, this OWT is found in open coastal waters as well as in the mid-water regions of river plumes.	SCC: 5.9 ± 8.0 mg L <sup>-1</sup> and SDD: 4.0 ± 2.3 m
Greenish-blue	Tertiary (WS6)	Tertiary’ (FU4-5)	Low-turbidity waters with slightly above ambient optically active constituent concentrations. In the GBR, this OWT is typical of GBR areas towards the open sea and include offshore regions of river plumes, fine sediment resuspension around reefs and islands and marine processes such as upwellings.	SCC: 3.9 ± 5.1 mg L <sup>-1</sup> and SDD: 7.0 ± 3.8 m
Blueish	Marine (WS7)	Marine’ (FU1-3)	Ambient waters with high light penetration and negligible levels of SSC, CDOM and Chl-a.	SCC: 2.2 ± 3.9 mg L <sup>-1</sup> and SDD: 11.1 ± 5.1 m

Eleven years (2009 to 2019) of daily MA Corrected Reflectance products (500-m resolution pixels) were processed with the WS colour algorithm. MA true-colour imagery was downloaded from the LANCE and EOSDIS (NASA) websites and corresponded to Rayleigh-corrected reflectance composites of MA bands 1, 4 and 3 (500-m resolution pixel). Images were processed using the WS colour algorithm, which includes: (1) a spectral enhancement function to transform Red-Green-Blue (RGB) images into Intensity-Hue-Saturation (HIS) and (2) a supervised classification method to cluster the enhanced pixels into “cloud” and the seven WS colour classes [48]. The supervised classification uses typical apparent surface colour signatures (RGB and HIS values) of wet season waters in the GBR, including under sun glint and light cloud conditions [48]. Discrimination of WS colour classes has been modified from the GBR wet season water body typology [64] and has been calibrated and validated with both satellite and historical in situ water quality data of the GBR [14,17]. The MA-WS products have been used in several recent environmental assessment studies in the GBR [65–68] and shown to be suitable for the Gulf of Papua-TS area in preliminary studies [27]. The 2009 to 2018 (10-years) MA-WS data were used in this study as the main satellite dataset to describe turbidity gradients in the Gulf of Papua-TS region. The full set of MA-WS data produced as part of this study is openly available in the TS EAtlas [69].

To verify colour patterns in the MA-WS maps, 1 year (2019) of Sentinel-3 Ocean and Land Colour Instrument (OLCI) Level 2 products (300-m resolution pixel) were downloaded on the EUMETSAT Data centre (hereafter S3). The data were processed into OWT maps using another colour scale—the Forel-Ule (FU) colour scale—a historical colour scale standard [50,56,70,71]. The FU colour scale divides water into 21 levels, ranging from dark blue to yellowish brown and was one of the earliest methods used to classify water masses into OWTs (Table 2). The 21 FU colour classes represent a wide range of optical characteristics of natural water bodies and can be used to assess the water colour of most inland and marine waters worldwide [71–73]. This choice was based on the findings of a recent case study focusing on the GBR [14] which showed that WS-equivalent OWTs maps can be produced by grouping the S3-FU colour classes 1–3 (equivalent to marine water type in the WS scale), FU colour classes 4–5 (equivalent to Tertiary water type in the WS scale), FU colour classes 6–9 (equivalent to Secondary water type in the WS scale) and FU colour classes  $\geq 10$  (equivalent to Primary water type in the WS scale) (Table 2). These classifications were adopted for the TS.

The S3 OLCI data were atmospherically corrected and processed with the FU Satellite Toolbox implemented in the Sentinel Application Platform (SNAP, [73]) to produce S3-FU water type maps of the study area. The FU satellite algorithm converts satellite normalised multi-band reflectance information into a discrete set of FU numbers using uniform colorimetric functions [70,71]. The derivation of the colour of natural waters is based on the calculation of Tristimulus values of the three primaries (X, Y, Z) that specify the colour stimulus of the human eye. The algorithm is validated by a set of hyperspectral measurements from inland, coastal and marine waters [70,71]. A selection of FU water-type maps of the study area in 2019 were reclassified into the four WS-equivalent OWTs (Table 2, Primary’, Secondary’ and Tertiary’ water types) and visually compared to MA-WS water type maps from 2019 to verify the validity of the GBR WS classification for the study area. A perfect equivalence between the MA-WS and S3-WS equivalent maps cannot be assumed, as MA and S3 satellite data are collected at different times of the day, from different optical satellites, and colour classes are processed using two different methods. However, the comparison was useful to determine whether colour patterns in the MA-WS maps were similar to the standard FU patterns in the atmospherically corrected S3 maps.

Finally, a selection of Sentinel-2 MSI/Multispectral Instrument (S2) high resolution true colour images of 2019 was extracted. S2 true colour images (10-m resolution pixel) were downloaded from the Sentinel-Hub EO Browser [74] and used in this study to illustrate turbidity and sediment transport in the TS area at a finer scale.

### 3.2. Water Quality Monitoring

Field data were periodically collected by several Australian scientific partners between 2016 and 2020 as part of the NESP-TWQ project [22,26,27,42]. The field campaigns were not focused on validating the satellite information, but rather on providing information on water quality characteristics and riverine discharge influences in the region and, therefore, were not necessarily collected close to the satellite overpass. Thus, a state-of-the-art validation of the MA-WS maps could not be performed, and the analyses of the field information were used instead to qualitatively support the satellite data and the satellite assessments in this study. Further details of sample collection, chemical analysis and data processing are provided in Appendix B and are fully described in [22,26,27,42].

#### (a) SSC measurements

Twenty-one surface SSC measurements were collected between 4 and 16 October 2016 across the whole TS region, and ten in situ SSC measurements were collected between 18 to 21 June 2018 around Saibai and Masig Island in the northern TS (Appendix B.1: Figure A2 and Table A1) [42]. SSC samples were acquired by filtering known volumes of water through pre-weighed 0.45 µm membrane filters (Millipore). The surveys aimed to estimate SSC concentrations across the whole TS, potentially linked to mine-derived pollution in marine waters [26,42]. This SSC dataset was used in this study to describe the composition of the OWT in the TS. The full set of data collected is openly available in the TS eAtlas [75,76].

#### (b) Optical dataset

A one-off collection of field FU colour, Secchi Disk Depth (SDD) and SSC measurements was conducted simultaneously at five sites in November 2020 around Saibai Islands in the northern western TS (Appendix B.2: Figure A3 and Table A2) [22]. Field FU colour class were measured with the Eye On Water (EOW) phone application developed in the European Citclops (Citizens' Observatory for Coast and Ocean Optical Monitoring) project. EOW allows users to collect FU water colour measurements from their smartphone cameras [50,77,78] and has been shown to be a robust application for capturing the FU colour of water with accuracy and precision [79]. SSC measurements were acquired using the same method as described above, and the SDD was measured using a standard 30 cm Secchi disk, lowering the disk in the water and measuring to what depth it was still visible [22]. SSC and SDD measurements were matched up with the EOW-FU data and were also used to describe the composition of the OWTs in TS.

#### (c) Salinity data

Surface salinity data were collected in the northern TS from February 2017 to early 2021 (Appendix B.3: Figure A4 and Table A3) [22,26]. Data were collected by local TS rangers using handheld salinity meters at Boigu, Saibai, Erub, Masig, Iama, Poruma and Warraber Islands (Figure 1, white circles). The monitoring program was designed to collect weekly salinity data and identify potential freshwater sources in the northern TS, but monitoring at some islands was more regular than others due to logistical constraints (ranging from 20 to 124).

#### (d) Continuous logger data

Continuous turbidity, salinity and temperature logger data were deployed at the northern end of the Warrior Reefs, located approximately 20 km from mainland PNG, from February 2020 to November 2020 (Figure 1, orange circle, and Appendix B.4: Table A4) [22]. The loggers included a Wet-Labs NTUS turbidity sensor and a SeaBird SBE-37 CTD, which collected continuous 10-min interval data over the 10-month period. The logger deployments were designed to collect data to the south-west of the Fly River mouth (approximately 60 km to the east of the site) and detect potential turbid freshwater sources coming from PNG mainland rivers. The full set of data collected is openly available in the TS eAtlas [80].

### 3.3. Data Analyses

#### 3.3.1. Spatial Analyses

MA-WS composite maps, including median (Table 3a), frequency (Table 3b) and difference (Table 3c) maps were produced using ArcMap 10.6 at different time scales (decadal (2009–2018), seasonal, and annual). They were used to illustrate turbidity gradients in the study area and assess TS areas and habitats exposed to turbid waters (“Turbidity Exposure”). The average long-term frequency of Primary, Secondary and Tertiary water types was mapped (Table 3b) and seasonal and monthly difference maps were used to describe relative changes in turbidity levels across seasons and months and illustrate the movements of turbid water masses (Table 3c).

**Table 3.** Satellite products used to describe turbid waters and habitat exposure in the Gulf of Papua-TS region. All products have been computed using daily MA-WS water type maps.

Product	Objective	Time Scales	Production
(a) Composite Colour class map	Illustrate large scale spatial patterns in turbidity levels at different time scales	Decadal (2009–2018)	Decadal median maps are produced by calculating the median long-term colour class category value for each pixel of our study area using (i) all daily MA-WS data using data from 2009 to 2018, or using data collected in the (ii) monsoon and trade wind seasons or (iii) in each month of the 2009–2018 period
(b) Frequency maps	Assess the area of coral reefs and seagrasses that were regularly exposed to turbid waters. Evaluate the frequency of exposure of TS coral reefs and seagrass key habitats to Primary, Secondary and Tertiary water types	Annual and decadal average	The annual water type frequency was defined as the total number of days per year exposed to a given water type divided by the number of data days (non-cloud) recorded per year, resulting in a normalised frequency on a scale from 0 to 1. Decadal average were calculated as the average of all annual frequency maps.
(c) Difference maps	Illustrate areas with an increase (positive anomaly) or decrease (negative anomaly) in relative turbidity during the trade wind season against the monsoonal trends; or in each month against long-term trends	Decadal seasonal or Decadal monthly	The seasonal difference map is calculated by subtracting the median decadal monsoonal and the median decadal trade wind maps. The monthly difference maps are calculated by subtracting the median decadal monthly maps and the decadal median map.

The long-term frequency maps were further used to assess the area of coral reefs and seagrasses that were regularly exposed to turbid waters, defined in this study as the combined Primary and Secondary water types (Table 3b). The assessment area is shown in Figure 1b and includes 2952 km<sup>2</sup> of mapped coral reefs and 1337 km<sup>2</sup> of mapped seagrass meadows. Exposure to each OWT was also assessed at several key sites across the region where habitat monitoring had been conducted in the past (shown in Figures 1 and 7) [26]. These sites were also regionally representative and included habitats of high ecological importance, including seagrass beds (west of Warrior Reef, Boigu Island) and coral reefs (Warrior Reef, Saibai, Ugar, Masig, Erub, Poruma and Mer Islands).

#### 3.3.2. Statistical Analyses

The SCC and optical field datasets were used to confirm that SSC and turbidity levels decrease (and SDD increase) from the Primary to the Tertiary WS water types in the study area. The MA-WS colour class category (WS1–7, Table 2) corresponding to the location and day of acquisition of each cloud-free SSC measurement collected in October 2016 and

June 2018 was extracted using ArcMap 10.6. The average SSC concentrations recorded in the MA-WS Primary, Secondary and Tertiary water types were then calculated. However, due to the high cloud cover in the study area, most surface SSC measurements collected in the field could not be matched with a MA-WS colour class category. The EOW-FU colour class category (FU 1-21, Table 2) and field SDD and SSC measurements collected in November 2020 were also matched up, and average SSC concentrations recorded in the S3-WS Primary', Secondary' and Tertiary' water types were calculated.

Time series and boxplots of salinity data collected in the northern TS were plotted and summary statistics calculated. The continuous turbidity, salinity and temperature logger data collected at northern Warrior Reef were averaged monthly and visualised in salinity-temperature and salinity-turbidity plots. Results were discussed against monthly patterns retrieved from the MA-WS water-type maps and used to identify patterns and the presence of freshwater influence in the TS ("Freshwater Influence"). Basic descriptive statistics were performed in Excel 2016.

### 3.3.3. Qualitative Assessment

The datasets described above were used together in a qualitative assessments to provide spatially explicit information for when and where the influence from Fly River discharge and/or derived sediments is likely to occur and to identify which TS ecosystems are the most likely to be exposed. The qualitative assessment was performed based on three indicators: "Turbidity Exposure", "Freshwater Influence" (as defined above) and the distance from the Fly River Delta ("Distance", in km). Distance was calculated as a straight-line length from the southern Fly River delta channel (8.8° S, 143.5° N) using Google Earth. The assessment was supported by additional evidence gained from the NESP-TWQ project and older reference literature. It was outside the scope of this paper to conduct a full assessment of the mine-derived pollution or of the ecological impact of Fly River discharges on TS ecosystems, even though recent data collected as part of the NESP-TSV project suggest it is likely to be limited [22,42].

## 4. Results

### 4.1. MODIS Water Type Maps

#### 4.1.1. Verification

WS colour patterns were very similar to the standard FU colour patterns, particularly for the Primary and Secondary water types, which confirmed the robustness and applicability of the GBR WS colour classification scheme to the study area (Figure 2). For example, large river plumes extending from the Fly River estuary and smaller turbid water masses adjacent to the Wassi Kussa and Mai Kussa Rivers were well defined and showed the same shapes, spatial areas and orientation on all example images. During the SE trade wind season, both satellites captured the punctual influence of the Fly River plume on Bramble Cay, the most north-eastern island of Australia located 55 kilometres SE of the mouth of the Fly River (Figure 2: 17 June and 31 August 2019). Another comparison of median composite maps for the January–April (monsoon season) and June–September (SE trade wind season) periods is available in Appendix C: Figure A5, which confirms the very similar patterns between the MA-WS and S3-FU products.

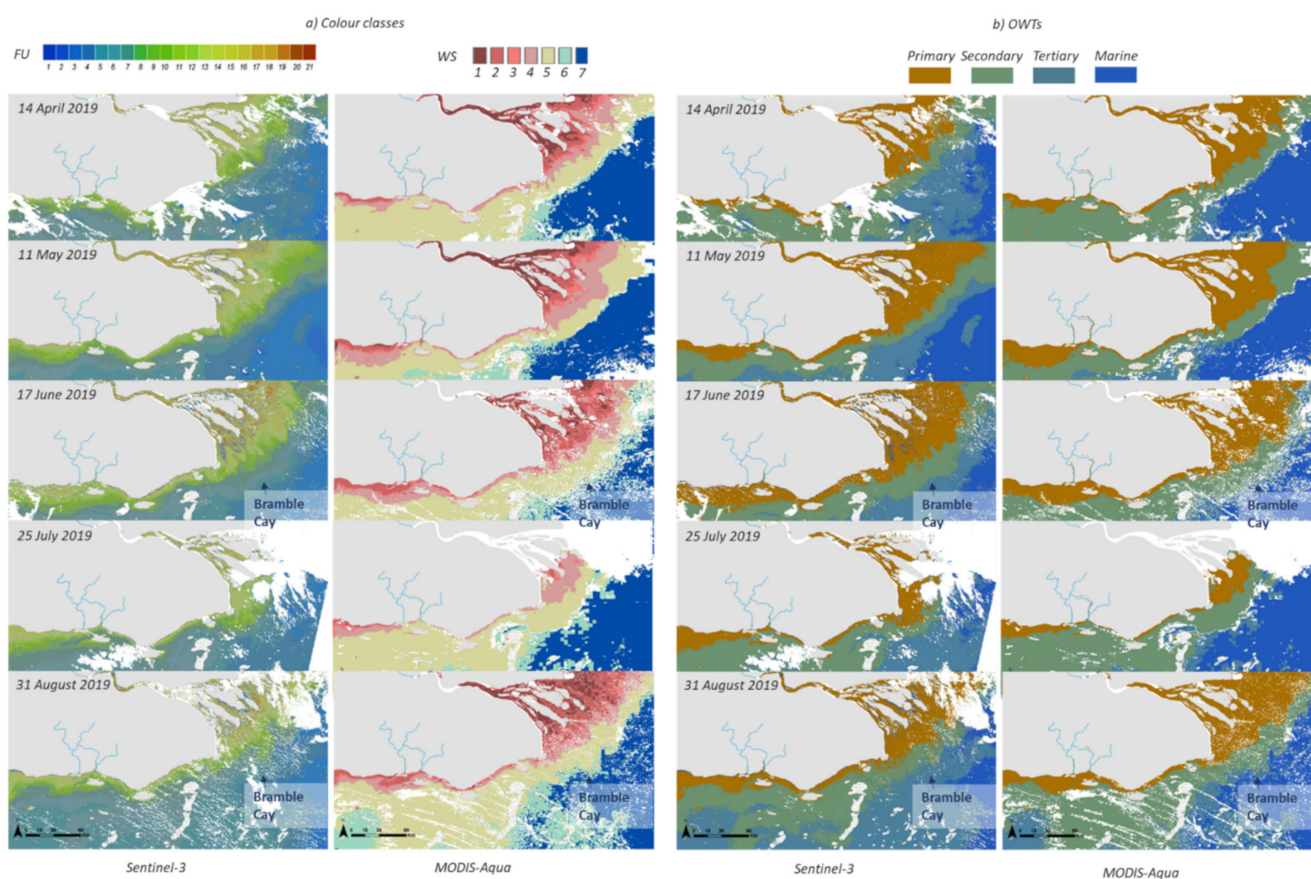


**Figure 2.** Examples of (a) colour class and (b) OWT maps produced with the Forel-Ule (FU) and Wet Season (WS) colour scales applied on Sentinel-3 and MODIS-Aqua optical imagery, respectively.

#### 4.1.2. Composition

MA-WS water-type maps of the study area were largely cloudy in the field surveys undertaken between 3 and 16 October 2016, except for the map from 12 October 2016, and MA-WS water-type maps were fully cloudy during the five days of the June 2018 survey [69]. Thirteen of the October 2016 samples could be matched up with the MA-WS water type maps and were all collected in the Secondary ( $n = 6$ ), Tertiary ( $n = 4$ ) and Marine ( $n = 3$ ) water types (Appendix B.1, Table A1). The mean field SSC across the MA-WS Secondary and Tertiary water types were consistent with long-term patterns documented in the GBR, i.e., SSC values decreased from the Secondary to the Tertiary water types (Figure 3a and Table 2). A comparison between EOW-FU measurements and the field SSC and SDD showed similar trends, i.e., SSC values decreasing from the Primary' to the Tertiary' water types (Figure 3b). SDD values logically increased from the Primary' to the Tertiary' water types (Figure 3b and Table 2).

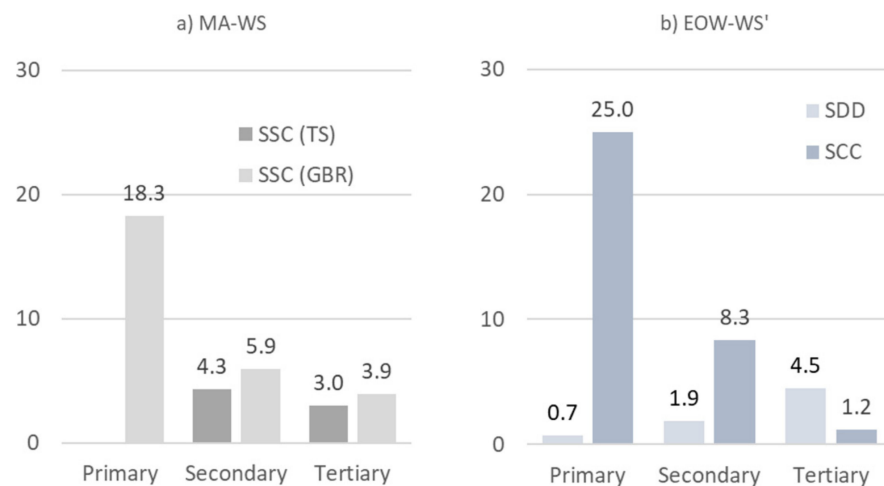


**Figure 3.** (a) Mean SSC measured in TS at the October 2016 survey sites (mg L<sup>-1</sup>, light grey and Appendix B.1) and mean long-term SSC documented for the GBR (data from [20], dark grey) across the MA-WS Primary, Secondary and Tertiary water types; (b) Mean SSC (mg L<sup>-1</sup>, dark blue) and SDD (m<sup>-1</sup>, light blue) measured in TS at the November 2020 survey sites across the EOW Primary', Secondary' and Tertiary' water types (Appendix B.2).

#### 4.1.3. Decadal Colour Patterns

In the median decadal MA-WS map, estuarine coastal waters along the southwest PNG coast were influenced by local river discharges entering the Gulf of Papua and typically classified as the turbid Primary water type (Figure 4a). In the Fly River Delta, the most turbid Primary waters (WS1–2) were mapped inside the shallow delta plains (the upper areas of the delta) and the colour classes changed from Primary to Tertiary water types moving further offshore from the Fly River Delta. The Secondary (WS5), less turbid water types covered a coastal band toward the open seas extending from the western TS to the north-eastern Gulf of Papua. This area included the northern region of the TS Protected Zone (Boigu and Saibai Islands), Daru Island and the northern Warrior Reefs (Figure 4b). The Tertiary water type (WS6, lower turbidity) was mapped further offshore and in the central TS, at the transition between coastal and marine ambient conditions.

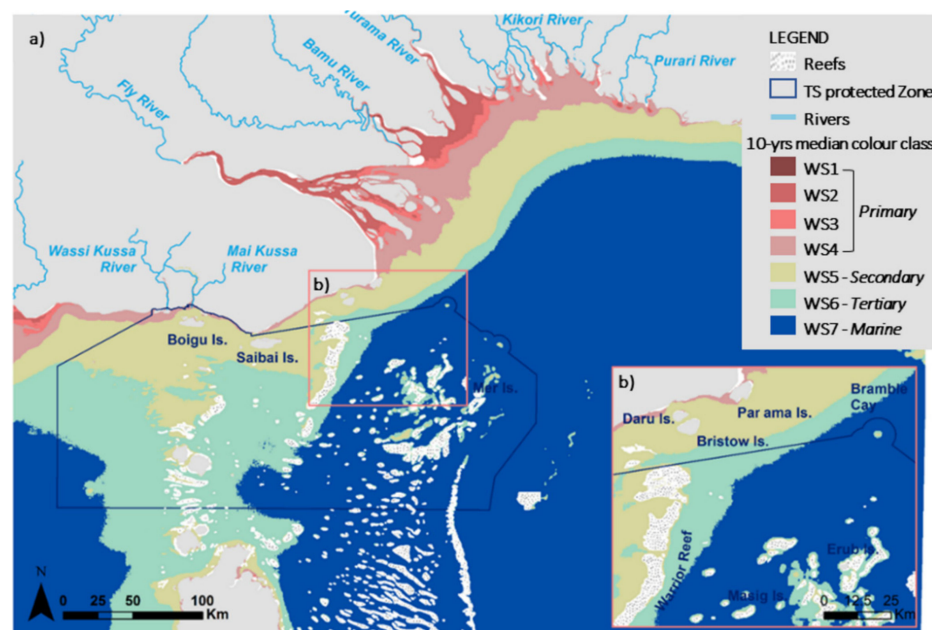


**Figure 4.** (a) Median decadal (2009–2018) colour class map illustrating long-term trends in turbidity levels in the study area, (b) Zoomed in map of Daru Island and the Warrior Reef ([22], modified).

#### 4.2. Seasonal Patterns

The decadal difference map illustrated the relative differences in water turbidity between the SE trade wind and monsoon season (Figure 5a). Higher relative turbidity levels were measured in the SE trade wind season than during the monsoon season off the Fly River delta and between Daru Island and Bramble Cay, including the north-eastern corner of the TS Protected Zone (Figure 5b). Higher relative turbidity levels were also measured along the southern PNG coast between Parama Island and Daru Island—even though the band of higher turbidity was patchy and restricted close to the coast—and west of Boigu Island in a large band along the southern PNG coast starting off at the Mai Kussa and Wassi Kussa river mouths. Conversely, the central TS was globally less turbid during the SE trade wind season than during the monsoon season in the decadal satellite database. Median decadal changes between the monsoon and SE trade wind season were often of one colour class category (see  $\Delta WS$  in Figure 5a), but the significance in terms of the change in turbidity value or SSC is unknown.

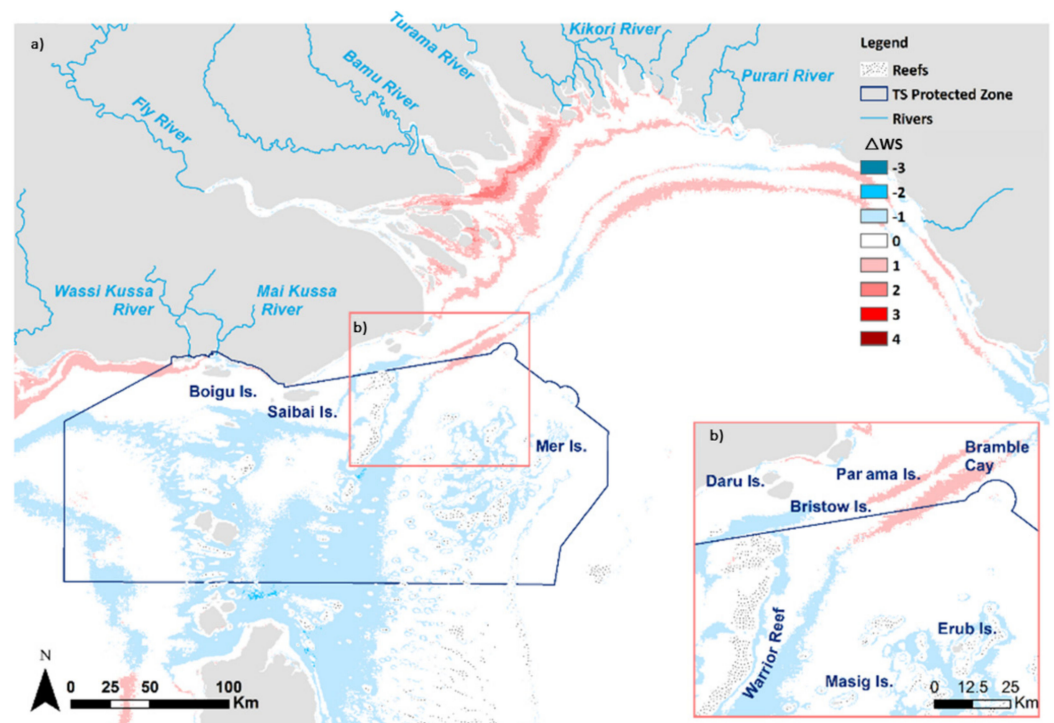


**Figure 5.** (a) Decadal seasonal difference map illustrating areas with an increase (red, positive turbidity anomaly) or decrease (blue, negative turbidity anomaly) in relative turbidity during the SE trade wind season against the monsoonal patterns. (b) Zoomed in map of Daru Island and the northern Warrior Reef. The seasonal difference map is calculated by subtracting the decadal median SE trade wind map to the decadal median monsoonal map (Table 3).  $\Delta WS$  is the difference in WS colour class category, with relative turbidity levels assumed to decrease from WS1 to WS7 ([22], modified).

The monthly difference maps provided a further assessment of the spatial patterns of the relative turbidity in the study area (Figure 6, the whole series presented in Appendix D: Figures A6 and A7). In the NE region of the TS, negative turbidity anomalies were mapped off the Fly River delta and around Bramble Cay and Parama Island during the monsoon season (Figure 6a and Appendix D: Figure A6). During the SE trade wind season, a positive turbidity anomaly developed from the Fly River estuary toward Bramble Cay, Parama Island, Daru Island and the Warrior Reefs (Figure 6b,c and Appendix D: Figures A6 and A7). Turbidity levels were relatively lower in the TS during the transition period, and negative anomalies were mapped between Daru Island and Bramble Cay (Figure 6d and Appendix D: Figure A7). In the middle of the TS, between the south of Boigu Island and the tip of

northern Australia, positive turbidity areas were localised east of the central islands in January and February (Figure 6a), in the middle of the central islands in May (Figure 6b) and then west of the central Islands in April to August (Figure 6c and Appendix D). These spatiotemporal patterns were in agreement with previous studies in the region that showed that prevailing currents are westward during the SE trade wind season and reversed eastward during the monsoon season (Table 1).

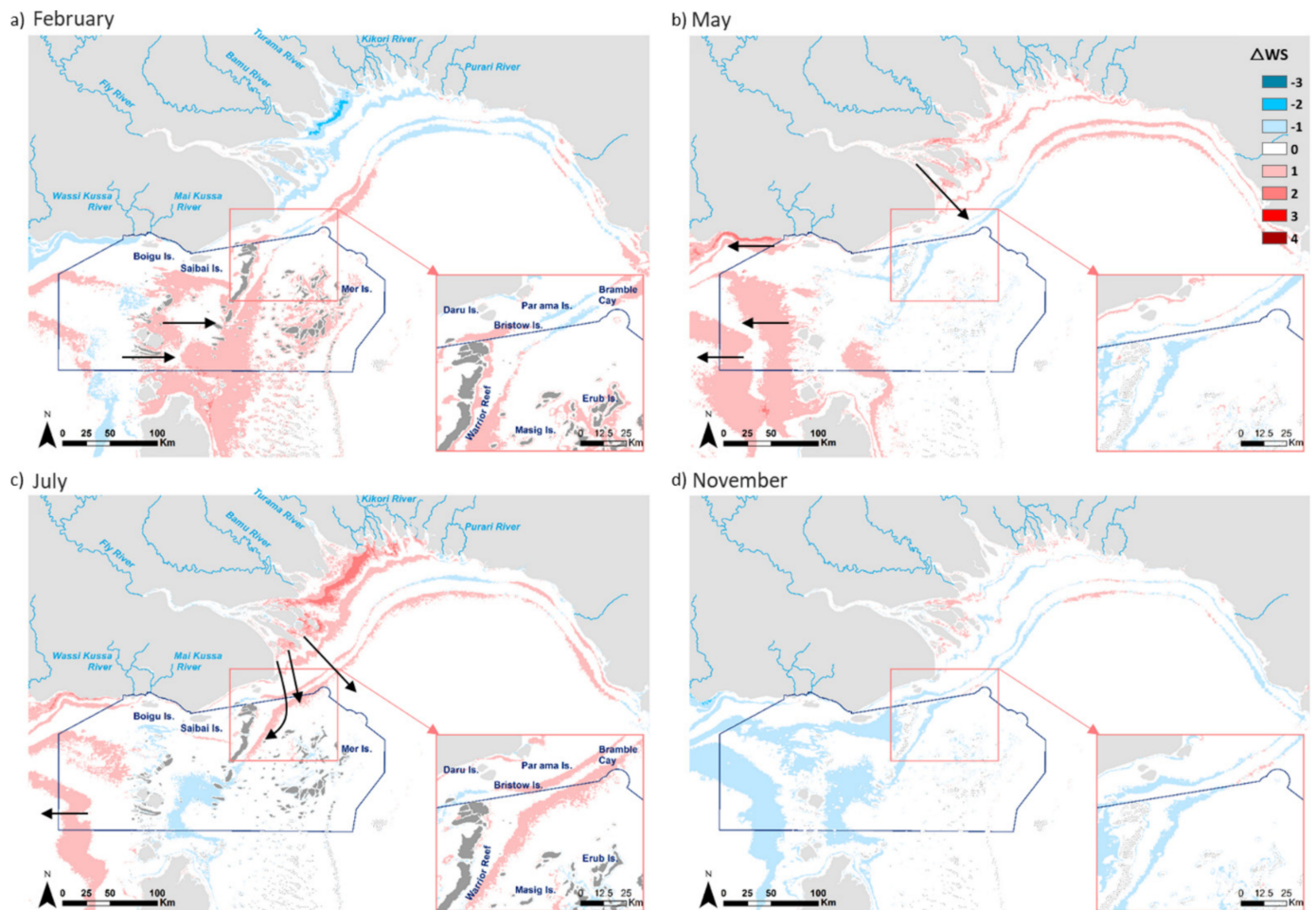


**Figure 6.** Decadal monthly difference maps illustrating areas with an increase (red, positive turbidity anomaly) or decrease (blue, negative turbidity anomaly) in turbidity in a selection of months relative to long-term patterns: (a) February, (b) May, (c) July and (d) November and zoom in map of Daru Island (bottom right corner). The monthly difference maps are calculated by subtracting the decadal median map (Figure 4) to the decadal median monthly maps (Table 3).  $\Delta WS$  is the difference in colour class category, with relative turbidity levels assumed to decrease from WS1 to WS7. Black arrows indicate tentative turbid water movement inferred from the difference maps ([22], modified). The whole series of monthly difference maps is available in Appendix D.

#### 4.3. Ecosystem Exposure to Turbid Waters

The multi-annual frequency maps (Figure 7A–C) illustrated the same inshore to offshore spatial pattern as the median decadal map (Figure 4), with the highest frequency of the Primary water type in the coastal areas, and offshore areas most frequently exposed to the Tertiary water type (Figure 7A–C). There was a limited area of coral reefs that were regularly exposed to turbid waters (the northern reefs), and 60% (or about 1700 km<sup>2</sup>) of the coral reef area was exposed to the Primary and Secondary water types infrequently (0–10% of the time, Figure 7). Intertidal and subtidal seagrass habitats had a greater exposure to turbid waters, with >50% (>150 km<sup>2</sup>) of intertidal and subtidal seagrass areas being

exposed to turbid waters 10–40% of the time. Satellite information was captured about 50% of the time in the study area (Figure 7D).

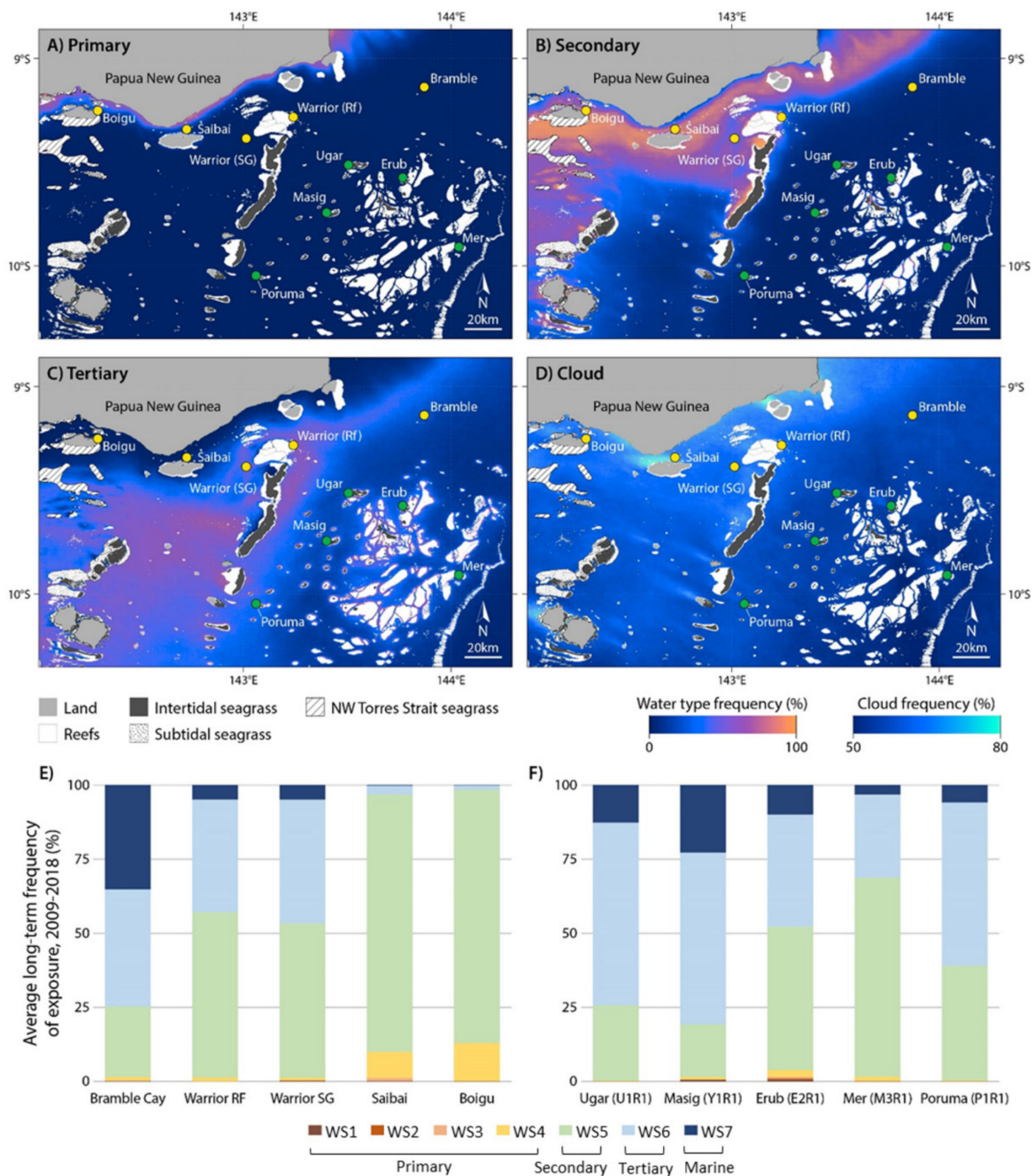


**Figure 7.** Maps showing the decadal (2009–2018) normalised frequency (0–100%) of (A) Primary water type (WS1–4), (B) Secondary water type (WS5) and (C) Tertiary water type (WS6), where the highest frequency is shown in orange, and the lowest frequency is shown in dark blue. (D) Cloud frequency occurrence, where the highest frequency is shown in light blue, and the lowest frequency is shown in dark blue. Bottom plots show the long-term frequency (% of exposure) extracted at a selection of key coral reef and seagrass monitoring sites in the TS: (E) northern sites (yellow dots) and (F) southern sites (green dot points) (extracted from [22]).

At the key habitat sites (Figure 7, yellow and green dots), exposure decreased from the most northern sites to the sites further south (Figure 7D,E). The greatest frequency of exposure to the Primary water type was measured at northern sites, including the Saibai and Boigu Islands (about 10% of the time on average), while Erub Island was the southern

site with the greatest exposure to the Primary water type (but <5% of the time). The Warrior Reef site and the Saibai, Boigu, Erub and Mer Island sites were predominantly exposed to the Secondary water type (WS5,  $\geq 50\%$  of the time), with the greatest frequency of exposure to the Secondary water type also measured at the Saibai and Boigu Islands (>80% of the time). The Ugar, Masig and Poruma Island sites were predominantly exposed to Tertiary waters (WS6,  $\geq 50\%$  of the time). Bramble Cay Island was exposed about 30% of the time to the Secondary and marine water types, 40% to the Tertiary, and rarely to the Primary water type.

#### 4.4. Freshwater Intrusions

The greatest numbers of salinity measurements collected as part of the weekly salinity monitoring program were at Warraber ( $n = 124$ ) and Masig Islands ( $n = 116$ ) (Figure 8a), and weekly salinity data were collected consistently throughout the monitoring period at these two locations (Appendix B.3: Figure A4). Sampling at Poruma ( $n = 69$ ) and Iama ( $n = 71$ ) was also relatively consistent but not as frequent, while sampling at Saibai ( $n = 51$ ) and Boigu ( $n = 28$ ) islands was irregular but increased in 2019 and 2020 (Appendix B.3, Figure A4).

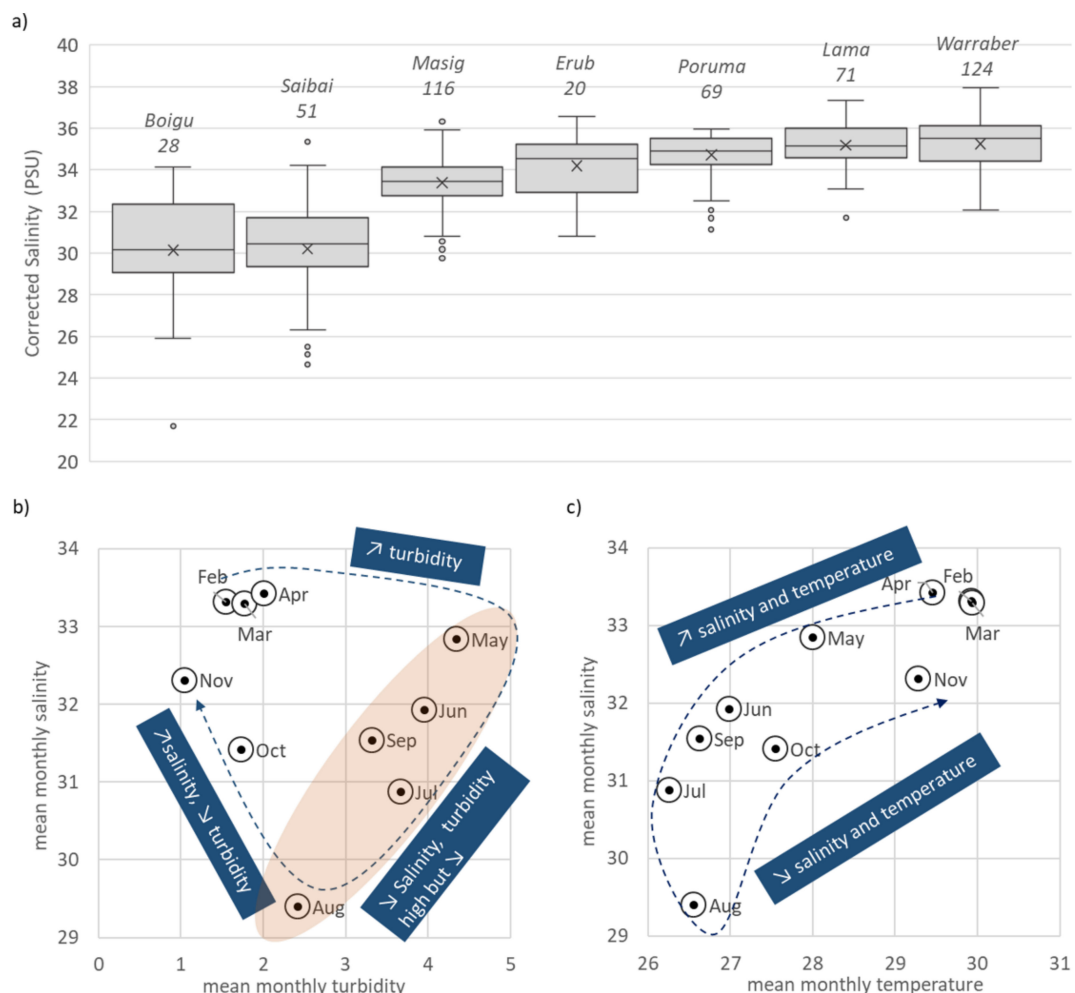


**Figure 8.** (a) Boxplots of the salinity measured at Boigu, Saibai, Masig, Erub, Poruma, Iama and Warraber Islands. Amount of data collected at each site is indicated (italic font). Bottom: Plots of the mean monthly logger data collected at the northern end of Warrior Reef in 2020 for (b) salinity-turbidity and (c) salinity-temperature ([22], modified). The red area highlights months with increased turbidity and decreased salinity levels that may indicate the influence of diluted riverine plume waters.

The lower mean salinities were measured at the most northern sites, Saibai Island ( $29.8 \pm 2.2$  PSU) and Boigu ( $30.1 \pm 2.6$  PSU), and these sites had the greatest salinity ranges (10.7 PSU and 12.4 PSU) (Figure 8 and Appendix B.3: Table A3). Inversely, the highest mean salinities were measured at the more southern sites, Warraber ( $35.3 \pm 1.2$  PSU), Iama ( $35.2 \pm 1.0$  PSU), and Poruma Islands ( $34.7 \pm 1.0$  PSU), and the lowest ranges were measured at Poruma (4.8 PSU), Iama and Erub (both 5.7 PSU). The mean salinity measurement at Masig Island was  $33.4 \pm 1.3$  PSU, and the range was relatively high (6.7 PSU). At this site, measurements were similar to average marine salinities but with the occasional reduction in salinity (to 33 PSU) in the SE trade wind season (Appendix B.3: Figure A4).

The mean monthly logger data collected at the northern Warrior Reef showed higher turbidity levels during the May–September period (Figure 8b and Appendix B.4, Table A3) than during October and November and the monsoon months (February to April:  $\leq 2$  NTU). The turbidity peak was measured in May (4.3 NTU), but the mean turbidity levels stayed relatively low ( $< 5$  NTU). The turbidity increase was accompanied by a gradual decrease in mean salinity (33.4 PSU in April to 29.4 PSU in August) and in mean temperature ( $29.5$  °C in April to  $26.3$  °C in July), which may indicate the influence of diluted turbid freshwaters around the northern Warrior Reefs (Figure 8b,c). Turbidity levels gradually decreased during the SE trade wind season (Figure 8a), which may reflect a winnowing of finer particles [37]. The 10 month average logger salinity, turbidity and temperature measured were  $32 \pm 2$  PSU,  $28 \pm 2$  °C and  $3 \pm 3$  NTU, respectively (in Appendix B.4: Table A3).

#### 4.5. Qualitative Assessment

Using the above satellite and field information, as well as the calculated distance from the Fly River Delta (“Distance”, in km, see Section 3.3.3), the area the most likely to be exposed to Fly River discharge and/or derived sediments was assessed to be located in NE corner of the TS and included, the north of Warrior Reefs (Zone 1), Bramble Cay (Zone 2) and Saibai and Boigu Islands (Zone 3) (Figure 9a, yellow symbols). Zones 1 and 3 were largely dominated by the Secondary water type, which indicated a regular occurrence of moderately turbid waters in this region of the TS (Figure 4). The habitats of the Boigu and Saibai Islands experienced the greatest exposure to turbid waters (Figure 7), and the Boigu and Saibai Islands had the lower salinity levels and the greatest salinity ranges (Figure 8a). The Boigu and Saibai Island were thus attributed the highest relative scores for both Turbidity Exposure and Freshwater Influence (Figure 9b, yellow symbols). Habitats around the northern Warrior Reefs were relatively less frequently exposed to turbid waters (Figure 7); however, the northern Warrior Reef is only 60 km SW of the Fly River delta and had relatively higher turbidity and lower salinity around the trade wind season in the 2020 logger data (Figure 8b). This likely indicates the influence of the diluted Fly River plume in the region. The Warrior Reef site was also attributed the highest relative scores for both Turbidity Exposure and Freshwater Influence, as well as for Distance (Figure 9, yellow symbols).

The source of both turbidity and brackish waters in zones 1 and 3 cannot be fully attributed to the Fly River plume and is likely to include other sources associated with the smaller streams, as well as resuspension of sediment deposited in the TS mud wedge via currents, wind and wave action (some of which may be derived from the Fly River plume). In particular, in Zone 3, the Fly River signature is likely to be diluted around Boigu Island, and the high turbidity levels measured there are most likely influenced by tidally resuspended sediments and the Mai Kussa and Wassi Kussa Rivers (Figures 4–7). However, further evidence in this area is required to confirm this, due to the location of Saibai and Boigu Island along the TS mud wedge, and despite their relative distance from the Fly River delta (Distance: 100 km and 150 km SW of the Fly River delta). Near the Fly River estuary, the transport of PNG sediment to the TS was particularly well illustrated by the S2 true colour image of 26 November 2019 (Figure 10c). In this image, terrigenous sediments from the Fly River were observed flowing westward through small passages between the

Panama/Daru Islands and the PNG coast, between Daru Island and Bristow Islands, and through Missionary Passage.

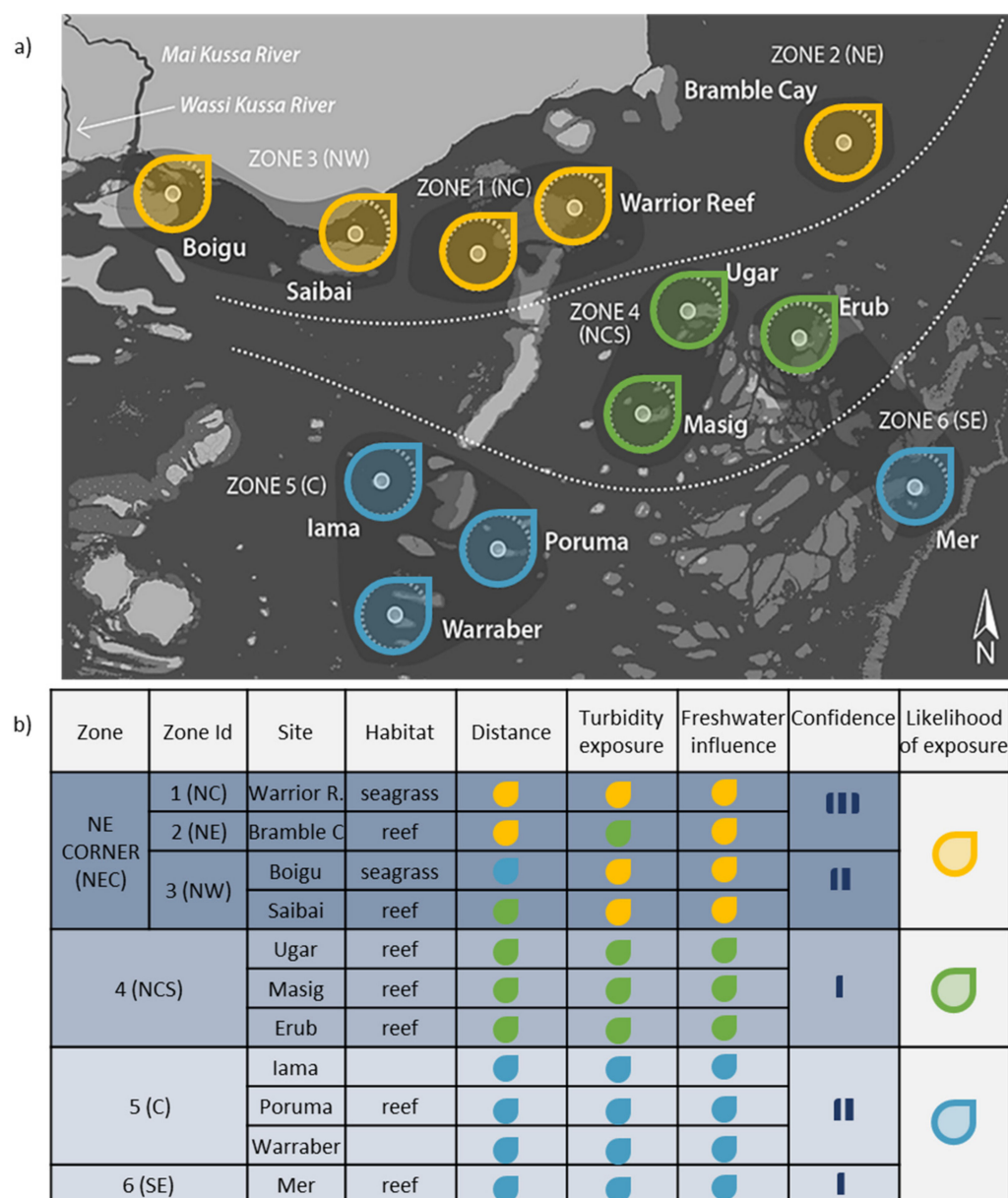


**Figure 9.** Quantitative assessment of the relative likelihood of exposure to Fly River discharge and/or derived sediments. (a) Map illustrating the different zones from the assessment, including the North-East Corner (NEC, zones 1 to 3), the North Central–South area (NSC, zone 4), the Central (C, zone 5) and the South-East (SE, zone 6) zones. (b) Table summarizing the sites and major habitats in each zone, the relative scores given to the three indicators used in the assessment: “Turbidity Exposure”, “Freshwater Influence” and “Distance”, and the final ‘likelihood of exposure’ score, where yellow–green–blue, indicate higher to lower relative scores.

Waters and habitats around Bramble Cay (Figure 9, Zone 2) were largely classified as the Tertiary or marine water type (Figures 4 and 7). However, previous studies have indicated that Bramble Cay has higher than expected levels of turbidity for a remote offshore reef [27]. Several satellite images in this study showed the Fly River plume reaching the Cay (for example, Figures 2 and 10d), and this appeared to be enhanced by SE trade wind environmental conditions (Figures 5 and 6). Luminescent lines have been observed in corals from Bramble Cay since 1781 [43], which, along with older observations [81], confirms

a freshwater influence attributed to the Fly River discharge at this site. Bramble Cay is located only 55 km SE of the mouth of the Fly River was attributed an average relative score for Turbidity Exposure, and a higher relative score for both Distance and Freshwater Influence. The instances of likely plume exposure at Bramble Cay were not fully resolved in this study, but exposure from the Fly River plume in this zone is likely.

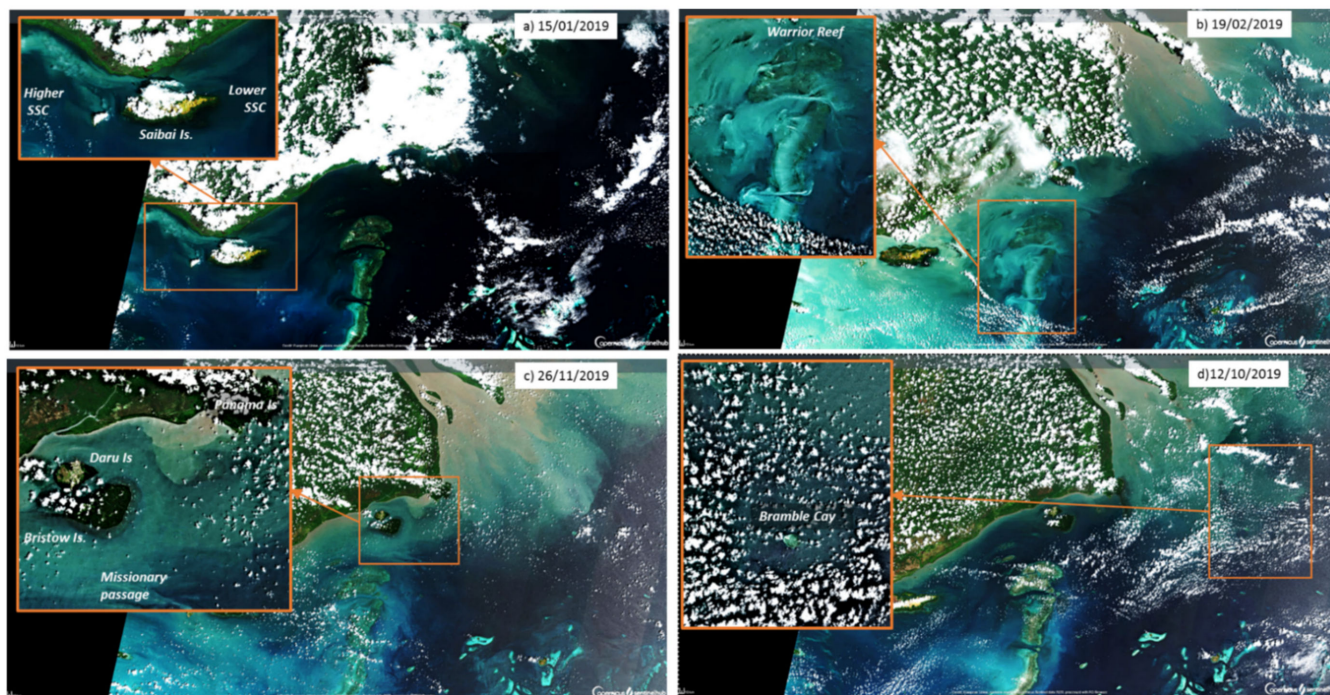


**Figure 10.** High resolution (10-m) S2 true colour images captured during the (top) monsoon and (bottom) trade wind seasons illustrating the very complex sediment circulation in the study area. (a) Typical monsoonal pattern with no sediment imports from the Fly River and higher SSC concentrations west of Saibai Island. Conversely, (b) shows high turbidity levels all along the PNG coast and in the middle of TS and is a great illustration of flow channelisation in passages among the Warrior Reefs. Trade wind image (c) illustrates complex sediment transport patterns near the coast and Fly River sediments flowing westward through passages between Panama and Daru Island and the PNG coast and through Missionary Passage, (d) a large Fly River plume reaching Bramble Cay, 55 kilometres SE of the mouth of the Fly River. Images are from the Sentinel-hub website and have been enhanced by +40% (brightness and contrast). Enlargements have been sharpened by 50% (extracted from [22]).

South of the NE corner, the North Central–South area (Zone 4, including Masig, Ugar and Erub islands) was classified as moderately likely to be exposed to Fly River discharge and/or derived sediments (Figure 9, green symbols). This zone was largely classified as being of the Tertiary or marine water types (Figure 4) and had higher salinity levels and smaller salinity variability (Figure 8a). However, the mean salinity measurement at Masig Island was lower than expected for an open ocean site (Figure 4a), and Erub and Masig Island were the southern sites with the greatest exposure to the Primary and Secondary water types (Figures 7 and 9b). Zone 4 was thus attributed an average relative score for turbidity exposure and Freshwater Influence. Due to the relative proximity of this zone to the mouth of the Fly River (Distance: 80 to 105 km), this zone was considered to be a transitional area and was therefore assessed as having a moderate relative likelihood of exposure.

Finally, the Central (Zone 5, including Iama, Warraber, Poruma) and South-East areas (Zone 6, Mer) were characterised as being less likely to be exposed to Fly River discharge and/or derived sediments (Figure 9, blue symbols). Both zones had limited or no evidence of Turbidity Exposure or Freshwater Influence influencing these areas and had the greater relative distance to the Fly River delta (Distance > 140 km S or SW of the Fly River delta). The Poruma, Lama and Warraber islands had the higher salinity levels and the lower salinity ranges. In these sites, the regular occurrence of the Tertiary water type (Figures 4 and 7) was likely due to the presence of suspended calcareous sediments originating from TS reefs and carbonate platforms [82], rather than any terrigenous influence. Zone 4 was thus attributed the lower relative scores for Freshwater Influence, Turbidity Exposure and Distance (Figure 9a).

Calcareous sediments are distinguishable from the riverine terrigenous sediments by their bright colour, as carbonate sediments are highly reflective in satellite visible bands (see for example Figure 10c,d). These calcareous sediments were stirred by currents, flowed through the Warrior Reef complex and sometimes mixed with the coastal terrigenous sediments, further complicating the colour signature around Boigu, Saibai and the northern Warrior Reefs (see for example Figure 10b). Seabed sediments comprised of mixed calcareous-siliciclastic sand and dominated by terrigenous phases have been sampled next to Saibai Island in a previous study [83]; which agreed with the above observations. There were no salinity data for Mer, and this site had a relatively high occurrence of Secondary waters and Tertiary waters in the frequency assessment (Figure 7B). This is unexplained but hypothesized to be linked either to the resuspension of carbonate sediments in this shallow zone or to bottom influence. Due to its location (Distance > 140 km S), Zone 6 was attributed a low relative score for all indicators, but there is a higher uncertainty in this specific assessment.

Confidence in the assessment varied for each zone and was maximum at Bramble Cay (Figure 9), where resuspension is likely to be minimum and the assessment supported by the historic coral cores [43], and at Warrior Reef, where several satellite images and the logger data supported the assessment. Data confidence was minimum in Zone 4 and Zone 6, where the number of observational data was limited.

## 5. Discussion

This study used a publicly available satellite time series and a colour classification algorithm originally developed for the GBR to map OWTs and turbidity gradients in the data-limited Gulf of Papua-TS region. The results were supported by field SSC, SDD and salinity measurements and used in a qualitative assessment to map TS areas and habitats the most likely exposed to Fly River discharge and/or derived sediments. The study demonstrated that methods using multiple datasets, including satellite imagery, are essential to qualitative exposure assessment in remote, complex and data-poor marine environments, such as the TS. Results complemented model simulations in the region over larger spatial and temporal frames, as well as previous sporadic observations in the region [23,41]. Despite the lack of field optical data in the TS, the colour-clustering approach used with the satellite data in this study provided large-scale and longer-term—but qualitative—observations and further insights on turbid water movements along the southern PNG coast. This approach allowed the identification of TS habitats that are the most likely to be exposed to Fly River discharge and/or derived sediments, as well as useful information for management applications.

No quantitative satellite estimates of SSC and turbidity were completed in this study, due to the insufficient amount of field data. However, the optical water type maps produced provided important information about water turbidity gradients in the study area, as well as information about their spatial and seasonal variability for the first time. The colour of waters is increasingly used as an efficient optical feature to cluster OWTs in both inland and marine waters and to assess water quality patterns and trends (e.g., [51–57]). This study reiterated the potential of using a qualitative colour clustering approach with satellite

images in large, complex and/or data-poor regions, where more classical quantitative remote sensing methods are limited by the lack of available field data. The methods used in this study can easily be transferred to other regions, using the now-available global colour-clustering algorithms and publicly available satellite data and processing tools, including the FU satellite and smartphone classification tools [50,54,71,73].

In the absence of a sufficient number of ground-truthing measurements, this study assumed that relative turbidity levels decreased from the Primary to the Tertiary water types in the TS, as observed in the GBR [14,17,20]. This assumption is expected to be reasonable, as good spatial agreement was observed between WS water type and standard FU water type composites (Figure 2), and water turbidity has been shown to increase with FU in global oceanic waters (measured as decreased Secchi disk depths and increased diffuse attenuation coefficient) [51]. The assumption was further supported by SSC and SDD measurements collected in the study area, as well as preliminary matchups with both satellite and smartphone water colour data (Figure 3).

Northern TS habitats contain complex and important seagrass and reef communities threatened by potential changes in water quality [35,84]. The satellite data provided a useful estimate of the spatial extent of habitats exposed to turbid waters and information about the frequency and seasonality of this exposure. On the scale of the whole of the TS, there was a limited area of coral reefs and seagrass habitats that were regularly exposed to turbid waters, except for the North-West TS seagrass area. However, this study provided sufficient cumulative evidence to reasonably assume that habitats located in the NE corner of the TS Protected Zone, including the northern Warrior Reef, as far west as Saibai Island and as far east as Bramble Cay, are likely the most exposed to Fly River discharge and/or derived sediments. Bramble Cay is a highly valued area of environmental and cultural significance [59] and is the largest nesting site for green turtles in the TS [85], as well as an important bird habitat area [86]. The surrounding waters are a major resource for the commercial mackerel fishery [87], which has recently shown sign of degradation [88]. The potential impact of the plume exposure in this region is currently unknown, and further studies would be required to ascertain potential links between the current environmental conditions and the Fly River discharge. Seagrass and reef habitats around the Boigu and Saibai Islands, and the Warrior Reef have high ecological and cultural value [62]. In particular, the extensive seagrass beds are an important food source for dugongs and turtles in the TS region [62].

Currents in the TS have been modelled to reverse seasonally, with their flow being predominantly westward during the SE trade wind season and eastward during the NW monsoon ([23,41,81] and Appendix A, Figure A1). This was further supported by the satellite water-type maps produced in this study, which mapped reversing turbid-water movement across the seasons (Figure 6). The Fly River plume intruded into the TS the most during the SE trade wind season and less during the monsoon season, in agreement with hydrodynamic and sediment modelling simulations in the region [23,41,81], as well as older field observations [31]. Satellite and mooring data at Warrior Reef suggested that, during the SE trade wind period, the intrusion into the TS Protected Zone could be greater between June and September, with a maximum around July–August (Figures 7 and 8), but further data should be collected to verify this assumption. Importantly, water quality campaigns as part of the larger NESP-TWQ project have shown that trace element concentrations were below the Australian and New Zealand marine water quality guideline values for 95% species protection in a selection of TS sites [22,42]. This suggests that, despite some intrusion of the Fly River discharge in the NE corner of the TS during the SE trade wind season, metal contamination of TS marine waters is limited and, overall, the water quality in the Torres Strait is good.

Around Boigu Island, turbid water masses off the Wassi Kussa and Mai Kussa Rivers also had higher relative turbidity levels around May to August, as well as a westward movement during this period (Figures 5 and 6). Flooding from the Mai Kussa River has been reported in the past [89], but its full contribution to the sediment budget in the NE TS has not been quantified in this or previous studies and requires further investigation. The satellite images reinforced that there is a turbid coastal boundary layer along the shallow PNG coast of the Torres Strait [23], and resuspension of sediment in this layer (some of which may derived from the Fly River plume) from strong tidal currents and winds also contributed to the elevated turbidity levels measured around Boigu and Saibai Island. In the monsoon season, the variability of the sediment fluxes has been attributed to storms and remote cyclone impacts [38]; and the very large turbid areas mapped in the high-resolution true-colour image of 26 November 2019 were likely related to storm-induced resuspension (Figure 10b). In this image, coastal terrigenous and offshore carbonate suspended sediments mixed in a large bright area, illustrating the optical complexity in the study area. Suspended carbonate sediments were observed flowing in passages among the Warrior Reef complex and around the more offshore reef, including the Ugar, Masig and Erub Islands. However, the waters were generally less turbid during the monsoon season in the NE corner of the TS (Figures 5 and 6), as illustrated by the high resolution S2 image of 15 January 2019 (Figure 10a).

The satellite images provided a highly valuable dataset at large scales and high temporal frequency, at no cost. There are, however, some limitations to their use. The dense cloud cover in the study area allowed satellite information to be captured about 50% of the time (Figure 7D), and it is likely that some large turbid plumes may have been missed. Furthermore, it was impossible to fully separate the direct riverine plume influence from wind, wave and tidally driven sediment resuspension in the satellite maps or to fully separate the calcareous from the terrigenous sediments on some images. It is acknowledged that resuspension, more particularly during the slack tide, has influenced the turbidity, and that other marine constituents, such as the chl-a or CDOM concentrations, may have influenced the colour gradients described in this study; even though this influence could not be quantified. However, the spatial and temporal trends in water composition described in this study were consistent with other evidences collected in the Gulf of Papua-TS region [22,23,26,39–43,81,82], suggesting that the cloud cover and above limitations did not substantially alter the data interpretation.

The preliminary validation exercises conducted as part of this study provided confidence in the colour and turbidity trends described (Figure 3), but the collection of additional field data would be essential to fully characterise the composition of the Primary, Secondary and Tertiary water types in the TS region. Measurements of local in situ SSC, turbidity and bio-optical properties of particulate and dissolved substances at different times of the year would allow the developing or testing of more complex satellite retrieval models, within or across the different OWTs, and the quantify turbidity levels (in NTU) and SSC (in  $\text{mg L}^{-1}$ ) in the study area. The remoteness of the study areas and high cloud cover, however, challenge the ability to collect in situ water-quality data concomitant to the satellite acquisition. The in situ logger salinity, temperature and turbidity data collected at Warrior Reef successfully supported the large-scale trends defined by the colour-class images. These types of continuous measurements might be more adapted in the remote and cloudy TS area to support the satellite information and current modelling effort in the region [23,41], as well as the parametrisation and/or validation of bio-optical algorithms for the study area. Particularly, long-term measurements at other key locations such as Boigu Island, Warrior Reef and around Daru Island would be highly valuable. Recent model predictions of sediment transport have shown that Panama, Daru and Bristow Islands form physical barriers that slow down the westward circulation of PNG sediments toward Saibai and Boigu Islands [23], which is supported by the high-resolution satellite data of the study area (Figure 10c). Accurate satellite estimates of SSC would allow calculating SS fluxes around those islands and further help calibrating and validating model simulations in the region.

However, even though the satellite classifications are subject to uncertainties, the satellite provided valuable and unique observations about the spatial and temporal variability of the turbidity in the study area for the first time. It provided spatially explicit information about linkages across terrestrial, freshwater and marine ecosystems and identified areas needing further investigation and/or where management effort should be focused. The results of this study were further combined with other information gathered in the northern TS, including in situ trace metal concentrations [42] and ecological data [62] into a more comprehensive risk assessment [22] and will be published in a future paper. This risk assessment process enhances our understanding of the potential impacts of the Fly River plume on the TS marine ecosystems and dependent communities. It can help managers in planning to mitigate the impacts of land-use change on water quality and coastal ecosystem services [90]. This is important for ensuring the protection of the Gulf of Papua-TS region given its importance to TS communities and turtle and dugong populations and its connectivity with the GBR Marine Park [62]. Finally, water colour is a very intuitive measure that helps to provide simple messages about water quality [14,50]. It has been used in TS community surveys as one parameter to describe change in water 'muddiness' with weather, temporal and geographical conditions [26]. Such information could be combined with the satellite data in the future. Community surveys provide local community members with the opportunity to share their knowledge and are essential to inform water quality management plans that are aligned with the community's water uses and values [91,92].

## 6. Conclusions

MODIS satellite data and a colour classification approach originally developed for the GBR were used to map OWTs and turbidity gradients in the data-limited Gulf of Papua-TS region. The publicly available satellite data were used in conjunction with available field measurements, as well as evidence from the literature to conduct a relative assessment of TS regions and habitats likely exposed to Fly River discharge and/or derived sediments. Results indicated that coastal habitats, including coral reefs and seagrass meadows, located as far east as Bramble Cay and as far west as Boigu Island, are located in the area that is most likely to be exposed, and that the Fly River influence there is enhanced during the SE trade wind season. This area is spatially limited relative to the scale of the TS region but encompasses habitat of high ecological importance. This study reiterated the potential of using a colour-clustering approach with satellite images to provide qualitative information on water quality in regions where more classical quantitative remote sensing methods are limited by the lack of available field data. It also demonstrated that methods using multiple sources of evidence, including satellite data, to conduct exposure assessments are essential in remote, complex and data-poor regions, such as the Torres Strait. While the satellite analyses presented in this study are qualitative and subject to uncertainties, they provide the long-term and spatially explicit baseline information needed to inform future ecological risk mapping and to support decisions about management priorities in the TS. They can easily be transferred to other regions using the now available global colour algorithms and freely distributed processing tools.

**Author Contributions:** Conceptualisation: C.P., J.W. and J.B.; Methodology, C.P., D.T. and E.W.; Validation, C.P.; Formal Analysis, C.P. and D.T., Investigation, C.P., D.T. and E.W., Writing: C.P. and J.W.; Visualization, C.P. and D.T.; Supervision, J.W. and J.B.; Funding Acquisition: J.W. and J.B. All authors have read and agreed to the published version of the manuscript.

**Funding:** This research was supported by the Australian Government National Environmental Science Program Tropical Water Quality Hub Project 5.14 (Identifying the water quality and ecosystem health threats to the Torres Strait from the Fly River runoff).

**Institutional Review Board Statement:** Not applicable.

**Informed Consent Statement:** Not applicable.

**Data Availability Statement:** Field data, environmental logger data and satellite images produced as part of this study are openly available in the Torres Strait EAtlas: <https://ts.eatlas.org.au/nesp-twq-5/ts-water-quality-5.14>, accessed on 8 April 2022. In making this data publicly available for management, the authors request being contacted and involved in any decision-making processes that incorporate this data, to ensure its methodology and limitations are fully understood. This study used several freely distributed satellite datasets: the MODIS imagery from the NASA Worldview application (URL: <https://worldview.earthdata.nasa.gov>, accessed on 8 April 2022), part of the NASA Earth Observing System Data and Information System (EOSDIS), the Sentinel-2 imagery from the Sentinel Hub EO browser (<https://www.sentinel-hub.com/explore/eobrowser/>, accessed on 8 April 2022) and the Sentinel-3 OLCI imagery from the EUMETSAT Copernicus Online Data (URL <https://codata.eumetsat.int/#/home/>, accessed on 8 April 2022).

**Acknowledgments:** This study was supported by the Australian Government’s National Environmental Science Program (NESP) Tropical Water Quality (TWQ) Hub and the Centre for Tropical Water and Aquatic Ecosystem Research (TropWATER) at James Cook University. In addition, the following people are thanked for providing field datasets for this study: Simon Apte (CSIRO), Scott Bainbridge (AIMS) and Jane Mellors (TropWATER). We would also like to thank the Torres Strait Regional Authority (TSRA) for their engagement in project activities and, in particular, the local Rangers for providing field support and undertaking local salinity monitoring. Finally, we would like to acknowledge our dear colleague Jon Brodie who passed away in 2020. Jon was instrumental in securing research funding for this and previous projects in the Torres Strait and the GBR. He was a strong science leader and a beloved mentor to many. The authors of this report appreciate the peer review comments provided by the anonymous reviewers whose inputs have provided valuable improvements to the paper.

**Conflicts of Interest:** The authors declare no conflict of interest.

## Abbreviations

Regions	
GBR	Great Barrier Reef Marine Park
PNG	Papua New Guinea
TS	Torres Strait
Satellites	
MA	MODIS-Aqua satellite
S3 or S2	Sentinel-3 or 2 satellites
Colour classification scales	
FU	Forel-Ule colour scale
WS	Wet Season colour scale
OWT	Optical Water types
Water quality parameters	
SSC	Suspended sediment concentrations
CDOM	coloured dissolved organic matters
Chl-a	chlorophyll-a
SDD	Secchi Disk Depth

## Appendix A. SLIM Model Outputs

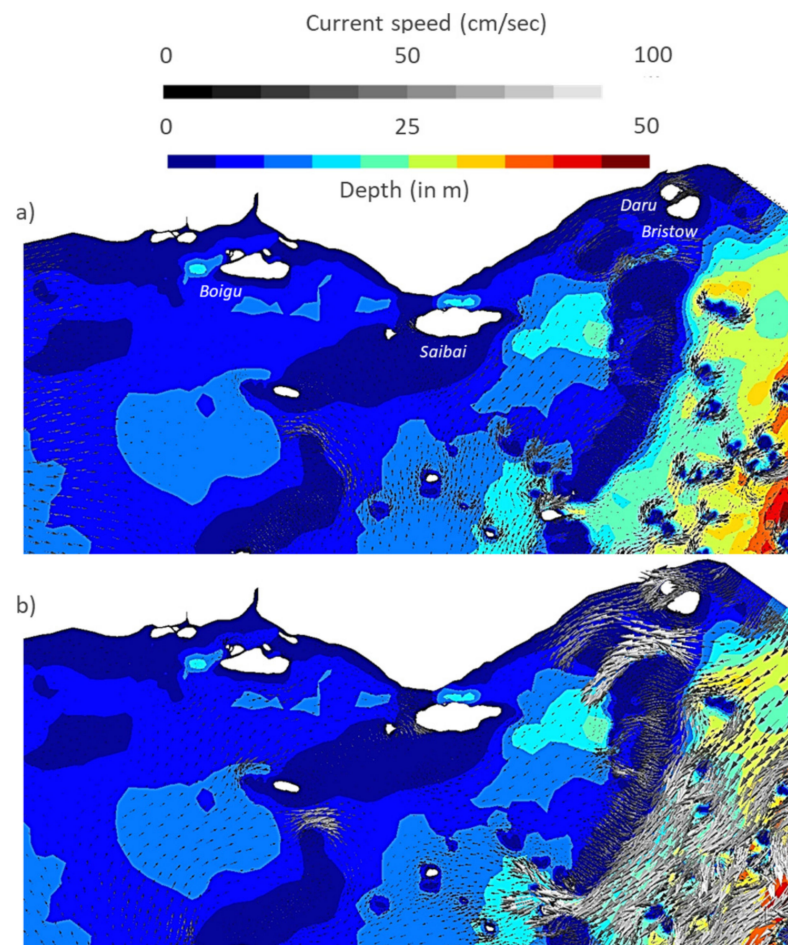


**Figure A1.** Tidally averaged currents under (a) monsoon wind (25 knots) and (b) strong SE winds (30 knots) modelled by the SLIM model ([23], unpublished data).

## Appendix B. Field Data

Field data were collected between 2016 and 2020 as part of a collaborative project aimed at identifying water quality and ecosystem health threats to the Torres Strait from Fly River runoff [22,26,27,42]. The field data used in this study to support the satellite assessment included:

### Appendix B.1. SSC Measurements

Suspended sediment samples for total SSC were acquired by filtering known volumes of water through pre-weighed  $0.45\ \mu\text{m}$  membrane filters (Millipore) in October 2016 (Figure A2a) and June 2018 (Figure A2b) [42]. The filters were rinsed with approximately 20 mL of deionised water to remove any salt and placed into acid-washed plastic Petri slides and stored frozen. The filters were oven-dried at  $60\ ^\circ\text{C}$ , cooled to room temperature in a desiccator and weighed. The SSC concentration (mg/L) of the water samples was calculated using the difference in the mass of the filter before and after filtration divided by the volume of sample filtered. The full set of data collected is openly available in the Torres Strait EAtlas [75,76].

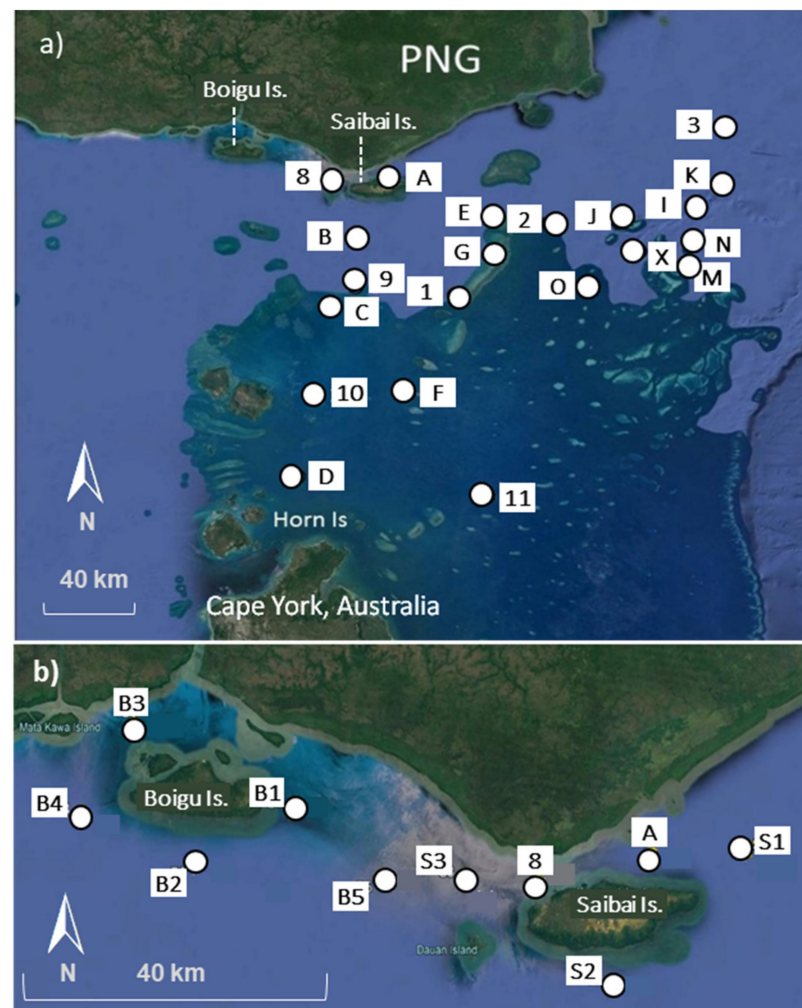


**Figure A2.** Map showing the locations of sampling sites (a) October 2016, (b) June 2018 ([26,42], modified). The background satellite image is from Google Earth.

**Table A1.** Water quality measured at the survey sites in October 2016 and June 2018 and corresponding MA-WS colour class (MA-WS, na = no data or clouds).

Sample ID	Date	SSC	Turbidity	MA-WS
Loc 1	3/10/2016	1.7	0.8	na
Loc G	3/10/2016	1.9	1.3	na
Loc 2	4/10/2016	2.5	0.6	7.0
Loc J	4/10/2016	2.3	0.4	na
Loc 3	5/10/2016	0.7	0.3	5.0
Loc K	5/10/2016	5.0	0.6	6.0
Loc I	5/10/2016	1.6	0.4	5.0
Loc M	6/10/2016	0.8	0.8	6.0
Erub	6/10/2016	1.1	0.6	5.0
Erub (duplicate)	6/10/2016	1.0	0.5	5.0
Loc X	7/10/2016	3.5	0.9	na
Masig	8/10/2016	0.6	0.4	na
Masig 2	8/10/2016	0.8	0.4	na
Site E	10/10/2016	7.3	2.7	na
Site 8	11/10/2016	12.0	8.8	na
Site A	11/10/2016	11.2	8.0	5.0
Site A (duplicate)	11/10/2016	10.4	8.0	5.0

**Table A1.** *Cont.*

Sample ID	Date	SSC	Turbidity	MA-WS
Site B	12/10/2016	4.8	2.1	6.0
Site 9	13/10/2016	3.0	2.0	na
Site C	13/10/2016	1.0	0.8	7.0
Site 10	13/10/2016	1.3	1.5	6.0
Site F	14/10/2016	1.1	1.7	7.0
Site 11	15/10/2016	1.8	1.5	na
Site D	16/10/2016	5.1	7.0	na
A	18/06/2018	13.3	na	na
S1	18/06/2018	4	na	na
S2	18/06/2018	6.1	na	na
8	18/06/2018	6.9	na	na
S3	18/06/2018	7.2	na	na
B3	18/06/2018	16.9	na	na
B4	18/06/2018	15.1	na	na
B5	21/06/2018	11.5	na	na

*Appendix B.2. Optical Dataset*

Field FU colour, Secchi Disk Depth (SDD) and SSC measurements were collected simultaneously at five sites in November 2020 around Saibai Island (Figure A3a and Table A2).

Field FU colour classes were measured with the Eye On Water (EOW) phone application and can be seen on the EOW website [77]. The FU colour-scale comparator is a 21-level colour classification system based on human visual comparisons with glass encased colour standards. It was developed in the late 19th century and can be used worldwide with any natural water body (marine, coastal, estuarine and lake ([54] and Figure A3b). The FU colour scale comparator has been implemented in a smartphone application in 2014: the EOW phone application as part of the European Citclops (Citizens' Observatory for Coast and Ocean Optical Monitoring) project. A phone camera is used to obtain above-water red, green and blue (RGB) images, and the water colour from digital images (WACODI) algorithm is used to extract the colour of natural waters from the digital images [50,77–79] (and Figure A3b). Retrieved data undergo a quality control procedure and are visualised on a map on the Citclops project website [77]. SSC measurements were acquired using the method described above, and the SDD was measured using a standard 30 cm white Secchi disk, lowering the disk in the water and measuring to what depth it is still visible.

**Table A2.** Secchi Disk Depth, SSC and Field FU measurements collected around Warrior Reef in November 2020 ([22], modified).

Sample ID	Date	Lat	Long	Secchi (m)	SSC (mg/L)	Field FU
S1	12/11/2020	−9.4	142.5	0.9	15	7
S2	12/11/2020	−9.4	142.6	0.7	25	15
S3	12/11/2020	−9.3	142.7	1.4	7.7	8
S4	12/11/2020	−9.3	142.9	3.4	2.3	6
S5	12/11/2020	−9.5	142.7	4.5	0.75	5
S5 Duplicate	12/11/2020	−9.5	142.7	4.5	1.6	5



**Figure A3.** (a) Map showing the location of field FU colour, Secchi Disk Depth and SSC measurements collected in November 2020 ([22], modified). FU scale measurements in the field using a Secchi Disc showing (b) the historical glass encased FU scale and (c) the FU-scale phone App. [50,77–79]. Map extracted and modified from the Eye on water website [54] and centred on Saibai Island (Figure 1 for the location of Saibai Island).

### Appendix B.3. Salinity Monitoring

Rangers from the Torres Strait Regional Authority (TSRA) were trained through the NESP project in 2016 to undertake a salinity monitoring program using handheld salinity and temperature meters [22,26]. Data were collected at Boigu, Saibai, Erub, Masig, Iama, Poruma and Warraber Islands (Figure 1), commencing at different times in 2017. The monitoring sites were located in at least 1 metre of water and were either located at the end of a jetty or off the beach.

The Rangers were advised not to locate the sites close to any land-based freshwater influence, such as a stream or discharge area, and to avoid periods of heavy rainfall [22,26]. The position of the sampling site was recorded using a GPS. Additional information including the date, time, estimate of the tide and the wind, and the collector's name and contact details was captured on the sample recording sheet. Outliers ( $n = 16$ ) were removed from the salinity database, and the time series of corrected data were plotted (Figure A4) and summary statistics calculated (Table A3). A full description of the data set is available in [22,26].

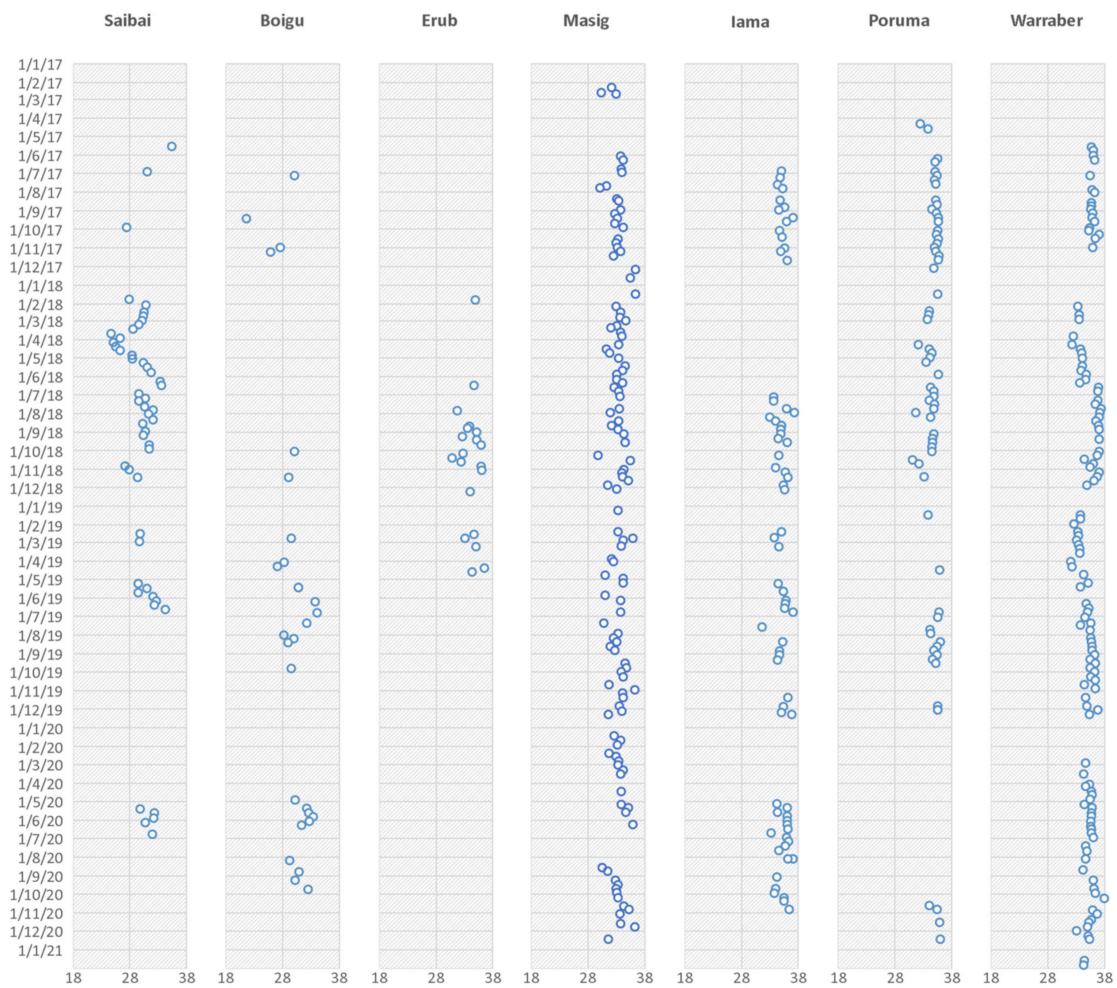


**Figure A4.** Time series of salinity measured at Saibai, Boigu, Erub, Masig, Iama, Poruma and Warraber Islands corrected salinity values (extracted from [22]).

**Table A3.** Summary statistics for the surface salinity measured at the Boigu, Saibai, Erub, Masig, Iama, Poruma and Warraber Islands (Figure 1) ([22], modified).

	Saibai	Boigu	Erub	Masig	Iama	Poruma	Warraber
count	51	28	20	116	71	69	124
mean	29.8	30.1	34.2	33.4	35.2	34.7	35.3
median	30.4	30.2	34.5	33.4	35.1	34.9	35.5
sd	2.2	2.6	1.5	1.3	1.0	1.0	1.2
min	24.6	21.7	30.8	29.8	31.7	31.1	32.1
max	35.3	34.1	36.6	36.4	37.3	36.0	37.9
range	10.7	12.4	5.7	6.7	5.7	4.8	5.9
Q1	29.4	29.1	33.0	32.8	34.6	34.3	34.4
Q3	31.6	32.3	35.2	34.1	36.0	35.5	36.1

#### Appendix B.4. Continuous Logger Data

A Wet-Labs NTUS turbidity sensor and a SeaBird SBE-37 CTD instrument were deployed at the Northern Warrior Reef to collect continuous turbidity, salinity and temperature data [22]. The instruments were deployed in February 2020 and recovered in

November. The data was downloaded and, using the manufacturer’s software, converted to standard units including accounting for calibration data. The data were topped and tailed to remove data when the instruments were not in the water (using the time stamps and depth sensor). Finally, the data were visually inspected and any spikes and other anomalous values removed. The full set of data collected is openly available in the Torres Strait EAtlas [80]. Continuous measurements were averaged monthly (Table A4, mean ± SD)

**Table A4.** Mean (±1 SD) salinity, temperature and turbidity measured at Warrior Reef in 2020 ([22], modified).

	Salinity (PSU)		Temperature (°C)		Turbidity (NTU)	
	Mean	SD	Mean	SD	Mean	SD
February	33.31	0.31	29.93	0.41	1.55	0.87
March	33.29	0.22	29.94	0.51	1.77	1.03
April	33.42	0.56	29.46	0.40	2.01	1.31
May	32.84	1.52	28.00	0.50	4.35	4.00
June	31.92	1.45	26.99	0.32	3.96	2.99
July	30.87	1.64	26.26	0.27	3.67	2.87
August	29.40	1.75	26.56	0.52	2.41	2.45
September	31.54	1.23	26.63	0.42	3.32	1.94
October	31.41	1.34	27.55	0.75	1.73	1.21
November	32.31	0.05	29.29	0.50	1.05	0.27
February–November	31.94	1.80	27.83	1.45	2.80	2.56

### Appendix C. Median Composites

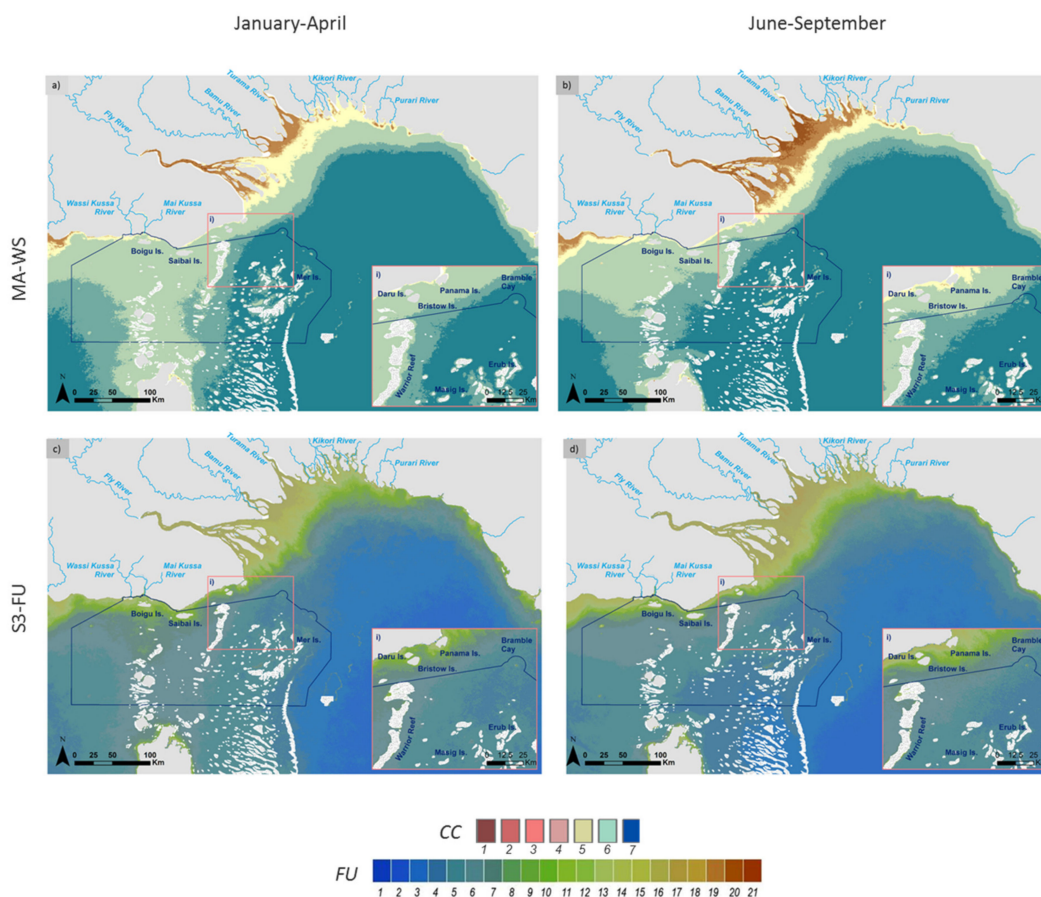


**Figure A5.** Median composite maps for the January–April (monsoon period) and June–September (SE trade wind season): (top) MA-WS (a,b) and (bottom) S3-FU composites (c,d).

## Appendix D. Decadal Monthly Difference Maps

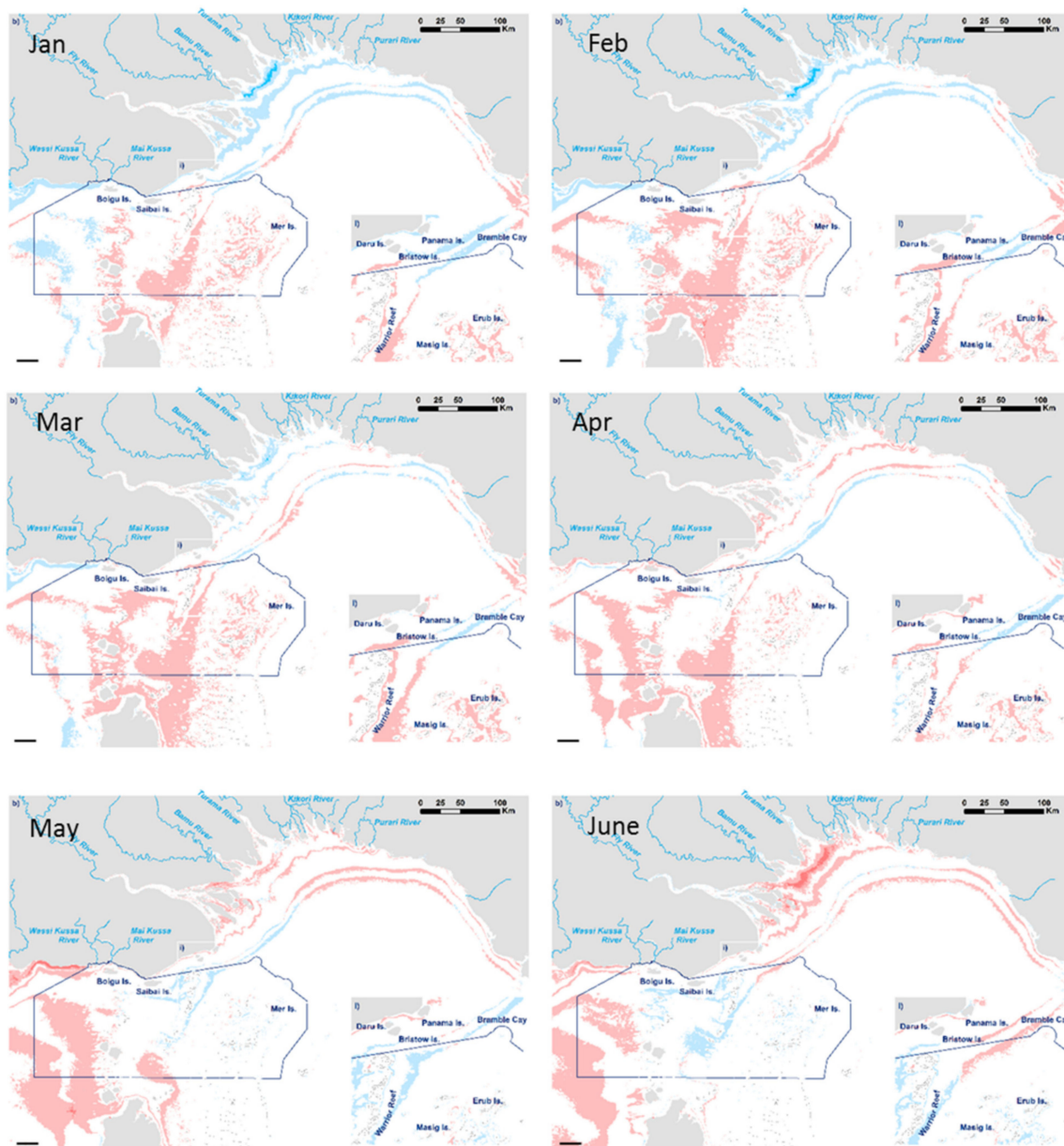


**Figure A6.** Decadal monthly difference maps illustrating areas with an increase (positive turbidity anomaly) or decrease (negative turbidity anomaly) in turbidity in each month relative to long-term trends: January to June. Reddish colours show areas with higher turbidity levels, blueish coloured areas have lower turbidity levels against the long-term trends. The monthly difference maps are calculated by subtracting the mean decadal monthly median maps (Table 3) and the decadal median map (Figure 4b), where an increase in colour class category means a positive turbidity anomaly (and inversely).

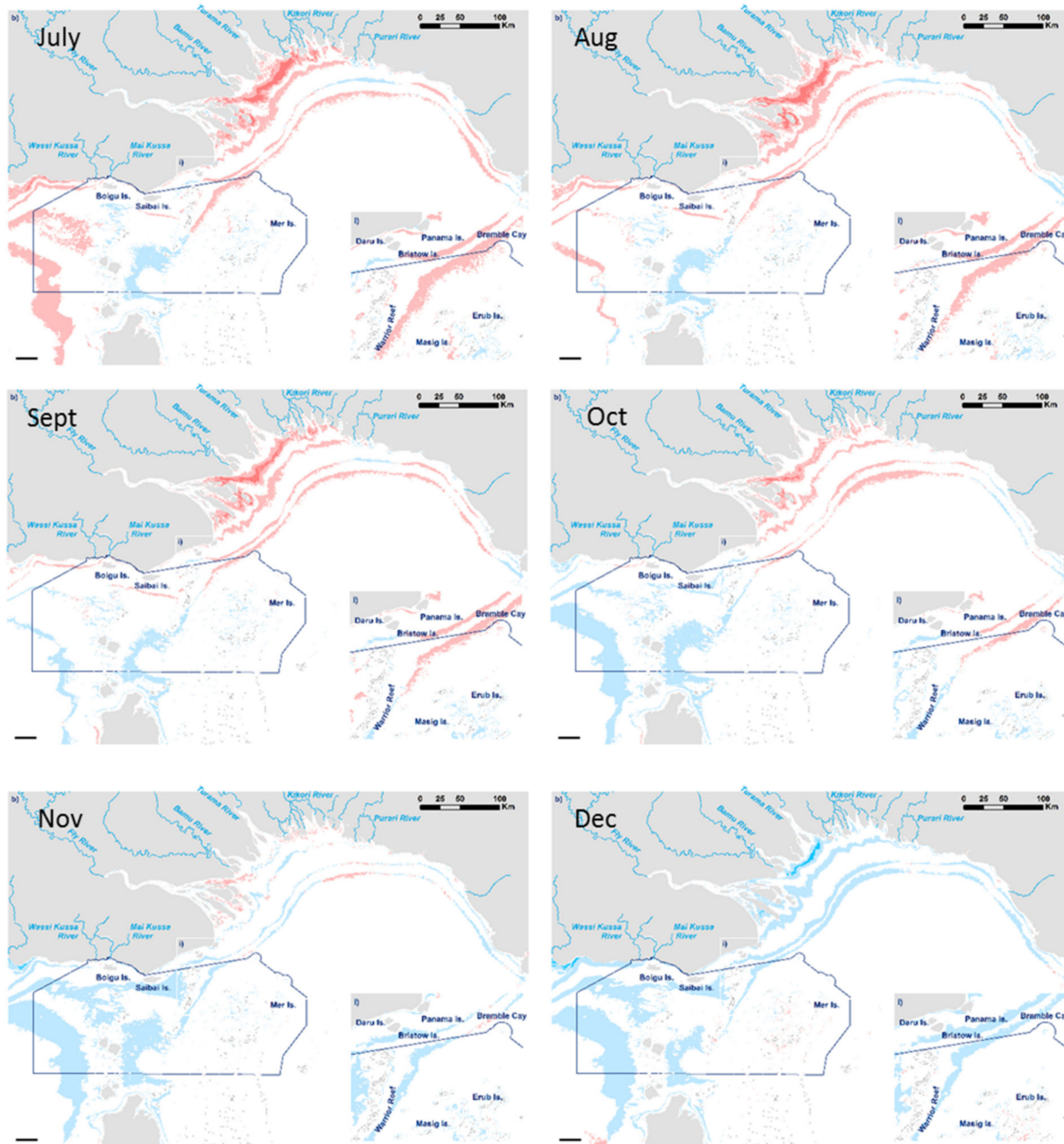


**Figure A7.** Decadal monthly difference maps illustrating areas with an increase (positive turbidity anomaly) or decrease (negative turbidity anomaly) in turbidity in each month relative to long-term trends: July to December. Reddish colours show areas with higher turbidity levels, blueish coloured areas have lower turbidity levels against the long-term trends. The monthly difference maps are calculated by subtracting the mean decadal monthly median maps (Table 3) and the decadal median map (Figure 4b), where an increase in colour class category means a positive turbidity anomaly (and inversely).

## References

- Halpern, B.S.; Frazier, M.; Potapenko, J.; Casey, K.S.; Koenig, K.; Longo, C.; Lowndes, J.S.; Rockwood, R.C.; Selig, E.R.; Selkoe, K.A.; et al. Spatial and temporal changes in cumulative human impacts on the world's ocean. *Nat. Commun.* **2015**, *6*, 7615. [[CrossRef](#)] [[PubMed](#)]
- Thrush, S.F.; Hewitt, J.E.; Cummings, V.J.; Ellis, J.I.; Hatton, C.; Lohrer, A.; Norkko, A.J.F.I.E. Muddy waters: Elevating sediment input to coastal and estuarine habitats. *Front. Ecol. Environ.* **2004**, *2*, 299–306. [[CrossRef](#)]

3. Romero, E.; Garnier, J.; Lassaletta, L.; Billen, G.; Le Gendre, R.; Riou, P.; Cugier, P. Large-scale patterns of river inputs in southwestern Europe: Seasonal and interannual variations and potential eutrophication effects at the coastal zone. *Biogeochemistry* **2013**, *113*, 481–505. [[CrossRef](#)]
4. Halpern, B.S.; Walbridge, S.; Selkoe, K.A.; Kappel, C.V.; Micheli, F.; D'Agrosa, C.; Bruno, J.F.; Casey, K.S.; Ebert, C.; Fox, H.E.; et al. A global map of human impact on marine ecosystems. *Science* **2008**, *319*, 948–952. [[CrossRef](#)]
5. Pockley, P. Global warming identified as main threat to coral reefs. *Nature* **2000**, *407*, 932. [[CrossRef](#)]
6. Wolff, N.H.; Mumby, P.J.; Devlin, M.; Anthony, K.R. Vulnerability of the Great Barrier Reef to climate change and local pressures. *Glob. Chang. Biol.* **2018**, *24*, 1978–1991. [[CrossRef](#)]
7. Brodie, J.; Lewis, S.; Collier, C.J.; Wooldridge, S.; Bainbridge, Z.; Waterhouse, J.; Rasheed, M.A.; Carol Honchin, C.; Holmes, G.; Fabricius, K. Setting ecologically relevant targets for river pollutant loads to meet marine water quality requirements for the Great Barrier Reef, Australia: A preliminary methodology and analysis. *Ocean Coast. Manag.* **2017**, *143*, 136–147. [[CrossRef](#)]
8. Klein, C.J.; Ban, N.C.; Halpern, B.S.; Beger, M.; Game, E.T.; Grantham, H.S.; Green, A.; Kelin, T.J.; Kinninmonth, S.; Treml, E.; et al. Prioritizing land and sea conservation investments to protect coral reefs. *PLoS ONE* **2010**, *5*, 12431. [[CrossRef](#)]
9. Brown, C.J.; Jupiter, S.D.; Albert, S.; Klein, C.J.; Mangubhai, S.; Maina, J.M.; Mumby, P.; Olley, J.; Stewart-Koster, B.; Tullock, V.; et al. Tracing the influence of land-use change on water quality and coral reefs using a Bayesian model. *Sci. Rep.* **2017**, *7*, 1–10. [[CrossRef](#)]
10. Maina, J.; de Moel, H.; Vermaat, J.E.; Bruggemann, J.H.; Guillaume, M.M.; Grove, C.A.; Madin, J.S.; Mertz-Kraus, R.; Zinke, J. Linking coral river runoff proxies with climate variability, hydrology and land-use in Madagascar catchments. *Mar. Pollut. Bull.* **2012**, *64*, 2047–2059. [[CrossRef](#)]
11. Petus, C.; Collier, C.; Devlin, M.; Rasheed, M.; McKenna, S. Using MODIS data for understanding changes in seagrass meadow health: A case study in the Great Barrier Reef (Australia). *Mar. Environ. Res.* **2014**, *98*, 68–85. [[CrossRef](#)]
12. Petus, C.; Teixeira da Silva, E.; Devlin, M.; Wenger, A.; Álvarez-Romero, J.G. Using MODIS data for mapping of water types within river plumes in the Great Barrier Reef, Australia: Towards the production of river plume risk maps for reef and seagrass ecosystems. *J. Environ. Manag.* **2014**, *137*, 163–177. [[CrossRef](#)]
13. Petus, C.; Devlin, M.; Thompson, A.; McKenzie, L.; Collier, C.; Teixeira da Silva, E.; Tracey, D. Estimating the Exposure of Coral Reefs and Seagrass Meadows to Land-Sourced Contaminants in River Flood Plumes of the Great Barrier Reef: Validating a Simple Satellite Risk Framework with Environmental Data. *Remote Sens.* **2016**, *8*, 210. [[CrossRef](#)]
14. Petus, C.; Waterhouse, J.; Lewis, S.; Vacher, M.; Tracey, D.; Devlin, M. A flood of information: Using Sentinel-3 water colour products to assure continuity in the monitoring of water quality trends in the Great Barrier Reef (Australia). *J. Environ. Manag.* **2019**, *2548*, 109255. [[CrossRef](#)]
15. Devlin, M.; Smith, A.; Graves, C.; Petus, C.; Tracey, D.; Maniel, M.; Hooper, E.; Kotra, K.; Samie, E.; Lyons, B. Baseline assessment of coastal water quality in Vanuatu, South Pacific: Insights gained from in-situ sampling. *Mar. Pollut. Bull.* **2020**, *160*, 111651. [[CrossRef](#)]
16. Painting, S.J.; Collingridge, K.A.; Durand, D.; Grémare, A.; Créach, V.; Arvanitidis, C.; Bernard, G. Marine monitoring in Europe: Is it adequate to address environmental threats and pressures? *Ocean Sci.* **2020**, *16*, 235–252. [[CrossRef](#)]
17. Devlin, M.; Petus, C.; Teixeira da Silva, E.; Tracey, D.; Wolff, N.; Waterhouse, J.; Brodie, J. Water Quality and River Plume monitoring in the Great Barrier Reef: An Overview of Methods Based on Ocean Colour Satellite Data. *Remote Sens.* **2015**, *7*, 12909–12941. [[CrossRef](#)]
18. Le Traon, P.Y.; Reppucci, A.; Fanjul, E.A.; Aouf, L.; Behrens, A.; Belmonte, M.; Bentamy, A.; Bertino, L.; Brando, V.E.; Kreiner, M.B.; et al. From observation to information and users: The Copernicus Marine Service perspective. *Front. Mar. Sci.* **2019**, *6*, 234. [[CrossRef](#)]
19. McCarthy, M.J.; Colna, K.E.; El-Mezayen, M.M.; Laureano-Rosario, A.E.; Méndez-Lázaro, P.; Otis, D.B.; Toro-Farmer, G.; Vega-Rodriguez, M.; Muller-Karger, F.E. Satellite remote sensing for coastal management: A review of successful applications. *J. Environ. Manag.* **2017**, *60*, 323–339. [[CrossRef](#)]
20. Waterhouse, J.; Gruber, R.; Logan, M.; Petus, C.; Howley, C.; Lewis, S.; Tracey, D.; James, C.; Mellors, J.; Tonin, H.; et al. Marine Monitoring Program: Annual Report for Inshore Water Quality Monitoring 2019–20. In *Report for the Great Barrier Reef Marine Park Authority*; Great Barrier Reef Marine Park Authority: Townsville, Australia, 2021; 200p.
21. Wolanski, E.; King, B.; Galloway, D. Dynamics of the turbidity maximum in the Fly River estuary, Papua New Guinea. *Estuar. Coast. Shelf Sci.* **1995**, *40*, 321–337. [[CrossRef](#)]
22. Waterhouse, J.; Apte, S.; Petus, C.; Bainbridge, S.; Wolanski, E.; Tracey, D.; Angel, B.M.; Jarolimek, C.V.; Brodie, J. NESP Project 5.14. Identifying water quality and ecosystem health threats to the Torres Strait from Fly River runoff. In *Report to the National Environmental Science Programme*; Reef and Rainforest Research Centre Limited: Cairns, Australia, 2021; 162p.
23. Wolanski, E.; Petus, C.; Lambrechts, J.; Brodie, J.; Waterhouse, J.; Tracey, D. The intrusion of polluted Fly River mud into Torres Strait. *Mar. Pollut. Bull.* **2021**, *166*, 112243. [[CrossRef](#)]
24. Angel, B.M.; Apte, S.C.; Simpson, S.L.; Jarolimek, C.V.; Jung, R.F. Behaviour of copper in the Fly River Estuary, Papua New Guinea. In *CSIRO Water for a Healthy Country Technical Report*; Prepared for Ok Tedi Mining Ltd.: Tabubil, Papua New Guinea, 2010; 45p.

25. Angel, B.M.; Apte, S.C.; Simpson, S.L.; Jarolimek, C.V.; King, J.J. The behaviour of trace metals in the Fly Estuary, Papua New Guinea. In *CSIRO Water for a Healthy Country Technical Report*; EP14897; Prepared for Ok Tedi Mining Ltd.: Tabubil, Papua New Guinea, 2014; 91p.
26. Waterhouse, J.; Petus, C.; Brodie, J.; Bainbridge, S.; Wolanski, E.; Dafforn, K.A.; Birrer, S.C.; Lough, J.; Tracey, D.; Johnson, J.E.; et al. NESP Project 2.2.1. Identifying water quality and ecosystem health threats to the Torres Strait and Far Northern GBR from runoff of the Fly River. In *Report to the National Environmental Science Programme*; Reef and Rainforest Research Centre Limited: Cairns, Australia, 2018; 162p.
27. Waterhouse, J.; Apte, S.C.; Brodie, J.; Hunter, C.; Petus, C.; Bainbridge, S.; Wolanski, E.; Dafforn, K.A.; Lough, J.; Tracey, D.; et al. Identifying water quality and ecosystem health threats to the Torres Strait from runoff arising from mine-derived pollution of the Fly River: Synthesis Report for NESP TWQ Hub Project 2.2.1 and NESP TWQ Hub Project 2.2.2. In *Report to the National Environmental Science Program*; Reef and Rainforest Research Centre Limited: Cairns, Australia, 2019; 19p.
28. Walsh, J.P.; Ridd, P.V. Processes, sediments, and stratigraphy of the Fly River Delta. In *The Fly River, Papua New Guinea: Environmental Studies in an Impacted Tropical River System, Developments in Earth & Environmental Sciences*; Bolton, B.R., Ed.; Elsevier: Burlington, MA, USA, 2009; Volume 9, pp. 153–176.
29. Wolanski, E.; Gibbs, R.J. Flocculation of suspended sediment in the Fly River estuary, Papua New Guinea. *J. Coast. Res.* **1995**, *11*, 754–762.
30. Harris, P.T.; Baker, E.K.; Cole, A.R.; Short, S.A. A preliminary study of sedimentation in the tidally dominated Fly River Delta, Gulf of Papua. *Cont. Shelf Res.* **1993**, *13*, 441–472. [[CrossRef](#)]
31. Wolanski, E.; Pickard, G.L.; Jupp, D.L.B. River plumes, coral reefs and mixing in the Gulf of Papua and the northern Great Barrier Reef. *Estuar. Coast. Shelf Sci.* **1984**, *18*, 291–314. [[CrossRef](#)]
32. O'Brien, D.; Mellors, J.; Petus, C.; Martins, F.; Wolanski, E.; Brodie, J. Monitoring and assessment of water quality threats to Torres Strait marine waters and ecosystems. In *Tropwater Report 15/43*; James Cook University: Townsville, Australia, 2015; 30p.
33. Petus, C. Application of MODIS remote sensing imagery for monitoring turbid river plumes from Papua New Guinea in the Torres Strait Region: A test study. In *Technical Report to the National Environmental Research Program*; Tropical System Hub: Cairns, Australia, 2013; 20p.
34. Lawrey, E.P.; Stewart, M. Mapping the Torres Strait reef and island features—Extending the GBR features (GBRMPA) dataset. In *Report to the National Environmental Science Programme*; Reef and Rainforest Research Centre Limited: Cairns, Australia, 2016; 117p.
35. Carter, A.B.; Taylor, H.A.; Rasheed, M.A. *Torres Strait Mapping: Seagrass Consolidation, 2002–2014*; JCU Publication, Report no. 14/55; Centre for Tropical Water & Aquatic Ecosystem Research: Cairns, Australia, 2014; 47p.
36. Carter, A.B.; Rasheed, M.A. Torres Strait Seagrass Long-term Monitoring: Dugong Sanctuary, Dungeness Reef and Orman Reefs. In *Centre for Tropical Water & Aquatic Ecosystems, Research Report No. 18/17*; James Cook University: Cairns, Australia, 2018; 35p.
37. Margvelashvili, N.; Saint-Cast, F.; Condie, S. Numerical modelling of the suspended sediment transport in Torres Strait. *Cont. Shelf Res.* **2008**, *28*, 2241–2256. [[CrossRef](#)]
38. Hemer, M.; Harris, P.T.; Coleman, R.; Hunter, J. Sediment mobility due to currents and waves in the Torres Strait–Gulf of Papua region. *Cont. Shelf Res.* **2004**, *24*, 2297–2316. [[CrossRef](#)]
39. Wolanski, E. A high resolution model of the water circulation in Torres Strait. In *NERP Project 4.4 Hazard Assessment for Water Quality Threats to Torres Strait Marine Waters, Ecosystems and Public Health*; Supplementary Report for NERP Project 4.4; James Cook University: Douglas, Australia, 2013; 45p.
40. Ogston, A.S.; Sternberg, R.W.; Nittrouer, C.A.; Martin, D.P.; Goni, M.; Crockett, J.S. Sediment delivery from the Fly River tidally dominated delta to the nearshore marine environment and the impact of El Niño. *J. Geophys. Res. Earth Surf.* **2008**, *113*, F01S11. [[CrossRef](#)]
41. Li, Y.; Martins, F.; Wolanski, E. Sensitivity analysis of the physical dynamics of the Fly River plume in Torres Strait. *Estuar. Coast. Shelf Sci.* **2017**, *194*, 84–91. [[CrossRef](#)]
42. Apte, S.C.; Angel, B.M.; Hunter, C.; Jarolimek, C.V.; Chariton, A.A.; King, J.; Murphy, N. Impacts of mine-derived contaminants on Torres Strait environments and communities. In *Report to the National Environmental Science Program*; Reef and Rainforest Research Centre Limited: Cairns, Australia, 2018; 126p.
43. Lough, J.M. Coral Core Records of the North-East Torres Strait. In *Report to the National Environmental Science Programme*; Reef and Rainforest Research Centre Limited: Cairns, Australia, 2016; 24p.
44. Balasubramanian, S.V.; Pahlevan, N.; Smith, B.; Binding, C.; Schalles, J.; Loisel, H.; Gurlin, D.; Greb, S.; Alikas, K.; Randla, M.; et al. Robust algorithm for estimating total suspended solids (TSS) in inland and nearshore coastal waters. *Remote Sens. Environ.* **2020**, *246*, 111768. [[CrossRef](#)]
45. Novoa, S.; Doxaran, D.; Ody, A.; Vanhellemont, Q.; Lafon, V.; Lubac, B.; Gernez, P. Atmospheric corrections and multi-conditional algorithm for multi-sensor remote sensing of suspended particulate matter in low-to-high turbidity levels coastal waters. *Remote Sens.* **2017**, *9*, 61. [[CrossRef](#)]
46. IOCCG. *Uncertainties in Ocean Colour Remote Sensing*; Mélin, F., Ed.; IOCCG Report Series, No. 18; International Ocean Colour Coordinating Group: Dartmouth, NS, Canada, 2019; 170p.
47. Toming, K.; Kutser, T.; Uiboupin, R.; Arikas, A.; Vahter, K.; Paavel, B. Mapping Water Quality Parameters with Sentinel-3 Ocean and Land Colour Instrument imagery in the Baltic Sea. *Remote Sens.* **2017**, *9*, 1070. [[CrossRef](#)]

48. Alvarez-Romero, J.; Devlin, M.; da Silva, E.; Petus, C.; Ban, N.; Pressey, R.; Kool, J.; Roberts, J.; Cerdeira-Estrada, S.; Wenger, A.; et al. A novel approach to model exposure of coastal-marine ecosystems to riverine flood plumes based on remote sensing techniques. *J. Environ. Manag.* **2013**, *119*, 194–207. [[CrossRef](#)]
49. Wang, S.; Li, J.; Zhang, W.; Cao, C.; Zhang, F.; Shen, Q.; Zhang, B. A dataset of remote-sensed Forel-Ule Index for global inland waters during 2000–2018. *Sci. Data* **2021**, *8*, 26. [[CrossRef](#)]
50. Ye, M.; Sun, Y. Review of the Forel–Ule Index based on in situ and remote sensing methods and application in water quality assessment. *Environ. Sci. Pollut. Res.* **2022**, *29*, 3024–13041. [[CrossRef](#)]
51. Pitarch, J.; van der Woerd, H.J.; Brewin, R.J.; Zielinski, O. Optical properties of Forel-Ule water types deduced from 15 years of global satellite ocean color observations. *Remote Sens. Environ.* **2019**, *231*, 111249. [[CrossRef](#)]
52. Fronkova, L.; Greenwood, N.; Martinez, R.; Graham, J.A.; Harrod, R.; Graves, C.A.; Devlin, M.J.; Petus, C. Can Forel-Ule act as a proxy of water quality in temperate waters? Application of the GBR work in the Liverpool Bay, UK. *Remote Sens.* **2022**; *in press*.
53. Chen, X.; Liu, L.; Zhang, X.; Li, J.; Wang, S.; Liu, D.; Duan, H.; Song, K. An Assessment of Water Color for Inland Water in China Using a Landsat 8-Derived Forel–Ule Index and the Google Earth Engine Platform. *IEEE J. Sel. Top. Appl. Earth Obs. Remote Sens.* **2021**, *14*, 5773–5785. [[CrossRef](#)]
54. Busch, J.A.; Bardaji, R.; Ceccaroni, L.; Friedrichs, A.; Piera, J.; Simon, C.; Thijsse, P.; Wernand, M.; Van der Woerd, H.; Zielinski, O. Citizen Bio-Optical Observations from Coast- and Ocean and Their Compatibility with Ocean Colour Satellite Measurements. *Remote Sens.* **2016**, *8*, 879. [[CrossRef](#)]
55. Li, J.; Wang, S.; Wu, Y.; Zhang, B.; Chen, X.; Zhang, F.; Shen, Q.; Peng, D.; Tian, L. MODIS observations of water color of the largest 10 lakes in China between 2000 and 2012. *Int. J. Digit. Earth* **2016**, *9*, 788–805. [[CrossRef](#)]
56. Wernand, M.R.; van der Woerd, H.J.; Gieskes, W.W.C. Trends in ocean colour and chlorophyll concentration from 1889 to 2000 worldwide. *PLoS ONE* **2013**, *8*, e63766. [[CrossRef](#)]
57. Wang, S.; Li, J.; Zhang, B.; Lee, Z.; Spyrakos, E.; Feng, L.; Liu, C.; Zhao, H.; Wu, Y.; Zhu, L.; et al. Changes of water clarity in large lakes and reservoirs across china observed from long-term MODIS. *Remote Sens. Environ.* **2020**, *247*, 111949. [[CrossRef](#)]
58. da Silva, E.F.F.; de Moraes Novo, E.M.L.; de Lucia Lobo, F.; Barbosa, C.C.F.; Cairo, C.T.; Noernberg, M.A.; da Silva Rotta, L.H. A machine learning approach for monitoring Brazilian optical water types using Sentinel-2 MSI. *Remote Sens. Appl. Soc. Environ.* **2021**, *23*, 100577.
59. Torres Strait Regional Authority. Land and Sea Management Strategy for Torres Strait 2016–2036. In *Report Prepared by the Land and Sea Management Unit*; Torres Strait Regional Authority: Thursday Island, Australia, 2016; 104p.
60. Sobotzick, S.; Hagihara, R.; Penrose, H.; Grech, A.; Cleguer, C.; Marsh, H. An assessment of the distribution and abundance of dugongs in the Northern Great Barrier Reef and Torres Strait. In *A Report for the Department of the Environment, National Environmental Research Program (NERP)*; Reef and Rainforest Research Centre Limited: Cairns, Australia, 2014; 73p.
61. Hamann, M.; Smith JPreston, S.; Fuentes, M.M.P.B. Nesting green turtles of Torres Strait. In *Report to the National Environmental Research Program*; Reef and Rainforest Research Centre Limited: Cairns, Australia, 2015; 13p.
62. Johnson, J.E.; Welch, D.J.; Marshall, P.A.; Day, J.; Marshall, N.; Steinberg, C.R.; Benthuisen, J.A.; Sun, C.; Brodie, J.; Marsh, H.; et al. Characterising the values and connectivity of the northeast Australia seascape: Great Barrier Reef, Torres Strait, Coral Sea and Great Sandy Strait. In *Report to the National Environmental Science Program*; Reef and Rainforest Research Centre Limited: Cairns, Australia, 2018; 81p.
63. Harris, P.T. Environmental Management of Torres Strait: A Marine Geologist’s Perspective. In *Gondwana to Greenhouse: Environmental Geoscience—An Australian Perspective*; Gostin, V.A., Ed.; Geological Society of Australia Special Publication: Adelaide, Australia, 2001; Volume 21, pp. 317–328.
64. Devlin, M.; Schaffelke, B. Spatial extent of riverine flood plumes and exposure of marine ecosystems in the Tully coastal region, Great Barrier Reef. *Mar. Freshw. Res.* **2009**, *60*, 1109–1122. [[CrossRef](#)]
65. Bainbridge, Z.; Lewis, S.; Stevens, T.; Petus, C.; Lazarus, E.; Gorman, J.; Smithers, S. Measuring sediment grain size across the catchment to reef continuum: Improved methods and environmental insights. *Mar. Pollut. Bull.* **2021**, *168*, 112339. [[CrossRef](#)]
66. Collier, C.J.; Carter, A.B.; Rasheed, M.; McKenzie, L.; Udy, J.; Coles, R.; Lawrence, E. An evidence-based approach for setting desired state in a complex Great Barrier Reef seagrass ecosystem: A case study from Cleveland Bay. *Environ. Dev. Sustain.* **2020**, *7*, 100042. [[CrossRef](#)]
67. Ceccarelli, D.M.; Evans, R.D.; Logan, M.; Mantel, P.; Puotinen, M.; Petus, C.; Russ, G.R.; Williamson, D.H. Long-term dynamics and drivers of coral and macroalgal cover on inshore reefs of the Great Barrier Reef Marine Park. *Ecol. Appl.* **2020**, *30*, e02008. [[CrossRef](#)]
68. Wenger, A.S.; Williamson, D.H.; da Silva, E.T.; Ceccarelli, D.M.; Browne, N.K.; Petus, C.; Devlin, M.J. Effects of reduced water quality on coral reefs in and out of no-take marine reserves. *Conserv. Biol.* **2016**, *30*, 142–153. [[CrossRef](#)]
69. Available online: <https://eatlas.org.au/data/uuid/95338405-4b6f-4093-b278-04039e884136> (accessed on 8 April 2022).
70. Wernand, M.R.; van der Woerd, H.J. Spectral analysis of the forel-ule ocean colour comparator scale. *J. Eur. Opt. Soc. Rapid Publ.* **2010**, *5*. Available online: [http://www.jeos.org/index.php/jeos\\_rp/article/view/322](http://www.jeos.org/index.php/jeos_rp/article/view/322) (accessed on 8 April 2022). [[CrossRef](#)]
71. Wernand, M.R.; Hommersom, A.; van der Woerd, H.J. MERIS-based ocean colour classification with the discrete forel-ule scale. *Ocean Sci.* **2013**, *9*, 477–487. [[CrossRef](#)]
72. Novoa, S.; Wernand, M.R.; Van der Woerd, H.J. The Forel-Ule scale revisited spectrally: Preparation protocol, transmission measurements and chromaticity. *J. Eur. Opt. Soc. Rapid Publ.* **2013**, *8*, 13057. [[CrossRef](#)]

73. Available online: <http://step.esa.int/main/toolboxes/sentinel-3-toolbox/s3tbx-features/> (accessed on 8 April 2022).
74. Available online: <https://www.sentinel-hub.com/explore/eobrowser/> (accessed on 8 April 2022).
75. Available online: <https://eatlas.org.au/data/uuid/c026de9e-bff4-4268-ad44-7c2e9bece110> (accessed on 8 April 2022).
76. Available online: <https://eatlas.org.au/data/uuid/03d84b70-d64c-4d89-846b-f1aa14f30ff7> (accessed on 8 April 2022).
77. Available online: <https://www.eyeonwater.org/observations> (accessed on 8 April 2022).
78. Novoa, S.; Wernand, M.R.; van der Woerd, H.J. Wacodi: A generic algorithm to derive the intrinsic color of natural waters from digital images. *Limnol. Oceanogr. Methods* **2015**, *13*, 697–711. [[CrossRef](#)]
79. Malthus, T.J.; Ohmsen, R.; Van der Woerd, H.J. An Evaluation of citizen science smartphone apps for inland water quality assessment. *Remote Sens.* **2020**, *12*, 1578. [[CrossRef](#)]
80. Available online: <https://eatlas.org.au/data/uuid/44eb7285-296f-4fe9-b662-46899364029e> (accessed on 8 April 2022).
81. Wolanski, E.; Lambrechts, J.; Thomas, C.; Deleersnijder, E. The net water circulation through Torres Strait. *Cont. Shelf Res.* **2013**, *64*, 66–74. [[CrossRef](#)]
82. Harris, P.T. Sediments, bedforms and bedload transport pathways on the continental shelf adjacent to Torres Strait, Australia—Papua New Guinea. *Cont. Shelf Res.* **1988**, *8*, 979–1003. [[CrossRef](#)]
83. Heap, A.D.; Scaffi, L. Composition and distribution of seabed and suspended sediments in north and central Torres Strait, Australia. *Cont. Shelf Res.* **2008**, *16*, 2174–2187. [[CrossRef](#)]
84. Gladstone, W. *Trace Metals in Sediments, Indicator Organisms and Traditional Seafoods of the Torres Strait*; Great Barrier Reef Marine Park Authority: Townsville, Australia, 1996; 177p.
85. Limpus, C.J.; Miller, J.D.; Parmenter, C.J.; Limpus, D.J. The Green Turtle, *Chelonia mydas*, Population of Raine Island and the Northern Great Barrier Reef: 1843–2001. *Mem. Qld. Mus.* **2003**, *49*, 349–440.
86. King, B.R. The Status of Queensland Seabirds. *Corella* **1993**, *17*, 65–92.
87. Begg, G.A.; Chen, C.C.M.; O’Neill, M.F.; Rose, D.B. Stock assessment of the Torres Strait Spanish mackerel fishery. *CRC Reef Res. Cent. Tech. Rep.* **2006**, *66*, 81.
88. Commonwealth of Australia. *Assessment of the Torres Strait Finfish Fishery*; Department of Agriculture, Water and the Environment: Canberra, Australia, 2020; 54p.
89. Marsh, H. Torres Strait Dugong 1998. In *Fisheries Assessment Report, Edited by the Torres Strait Fisheries Assessment Group*; Australian Fisheries Management Authority: Canberra, Australia, 1999; 23p.
90. Brown, C.J.; Jupiter, S.D.; Albert, S.; Anthony, K.R.; Hamilton, R.J.; Fredston-Hermann, A.; Halpern, B.S.; Lin, H.-Y.; Maina, J.; Mangubhai, S.; et al. A guide to modelling priorities for managing land-based impacts on coastal ecosystems. *J. Appl. Ecol.* **2019**, *56*, 1106–1116. [[CrossRef](#)]
91. Bohnet, I.C.; Kinjun, C. Community uses and values of water informing water quality improvement planning: A study from the Great Barrier Reef region, Australia. *Mar. Freshw. Res.* **2009**, *60*, 1176–1182. [[CrossRef](#)]
92. Kaiser, B.A.; Hoeberechts, M.; Maxwell, K.; Eerkes-Medrano, L.; Hilmi, N.; Safa, A.; Horbel, C.; Juniper, S.K.; Roughan, M.; Theux Lowen, N.; et al. The importance of connected ocean monitoring knowledge systems and communities. *Front. Mar. Sci.* **2019**, *6*, 309. [[CrossRef](#)]